TOWARDS A BETTER REPRESENTATION OF THE SUBSURFACE ACROSS THE CONTINENTAL US: DEVELOPING HYDRAULIC CONDUCTIVITY DATASETS FOR INTEGRATED HYDROLOGIC MODELS

By

Rachel S Corrigan

A thesis submitted to the Faculty and the Board of Trustees of the Colorado School of Mines in partial fulfillment of the requirements for the degree of Master of Science (Hydrology).

Golden, Colorado

Date _____

Signed: _____
Rachel S. Corrigan

Signed: _____
Dr. Reed M. Maxwell
Thesis Advisor

Golden, Colorado
Date _____

Signed: _____
Dr. Jonathan Sharp
HSE Program Director

ABSTRACT

Groundwater is the largest source of accessible freshwater, accounts for over 30% of total water use worldwide, and is intrinsically connected to land-surface processes. Groundwater flow is largely influence by hydraulic gradients and the properties of the porous media, such as hydraulic conductivity. The methods by which hydraulic conductivity is measured vary greatly among local, regional, and global scale measurements. Local-scale measurements can be made through borehole tests, and large-scale conductivity values are regularly regarded as the geometric mean of local-scale measurements. Effective conductivity values vary greatly with scale, leading to uncertainty in aggregated representations. Borehole and survey data gaps exist spatially which further exacerbated observational data limitations for informing aggregated estimates. This creates a scale dependent challenge that relies upon a variety of data types, each with its own inherent limitations.

The work presented here improves current regional permeability estimations by developing a new continental-scale hydraulic conductivity product. A previously published approach for estimating hydraulic conductivity from morphologic patterns was adapted and extended to the continental US. The geometric mean value from the new hydraulic conductivity product are comparable to existing continental-scale datasets. The density distribution of values from the new product shows less bimodality than other products, though exhibits an East-West trend. This indicates that the methodology captures more heterogeneity in conductivity values than other methods. The product developed here joins a growing number of products that improve our hydrologic understanding of North America. It will serve as a community resource for populating large scale models which will improve our understanding of how water flows through the Earth's crust.

TABLE OF CONTENTS

ABSTRACT ii

LIST OF FIGURES vi

LIST OF TABLES vii

CHAPTER 1 INTRODUCTION 1

CHAPTER 2 BACKGROUND 3

2.1 Groundwater Sustainability and Demand 3

2.2 Subsurface Characterization 5

2.3 Global and Continental Hydrologic Models 8

CHAPTER 3 METHODS 12

3.1 Estimating hydraulic conductivity using watershed geomorphology 12

3.1.1 Valley depth (d) 13

3.1.2 Drainage density (D) 14

3.1.4 Recharge (R) 15

3.1.5 Hydraulic Conductivity (K) 17

3.2 USGS Primary Aquifers and Secondary Hydrogeologic Regions 19

CHAPTER 4 RESULTS 21

4.1 Morphology Method Results 21

4.2 Comparison of Datasets 25

CHAPTER 5 DISCUSSION 28

CHAPTER 6 CONCLUSIONS 32

REFERENCES 34

APPENDIX A WATER TABLE DEPTH ACROSS THE HIGH PLAINS..... 40

APPENDIX B ESTIMATING CONDUCTIVITY OVER THE HIGH PLAINS..... 44

APPENDIX C INPUTS FOR K ESTIMATE ACROSS THE CONTINENTAL US..... 47

LIST OF FIGURES

Figure 3.1: Conceptual model showing geomorphology parameters: drainage density of the watershed (D), valley depth (d), recharge (D), and aquifer thickness (H). 12

Figure 3.2: The relationship between K and each of its parameters using Equation 3.3. 19

Figure 4.1: Density distribution of all variables used to calculate hydraulic conductivity. 22

Figure 4.2: Hydraulic conductivity (K) values [m/s] estimated using the adapted morphology method at subwatershed (HUC12) resolution. 23

Figure 4.3: Results of the four different K estimates using the adapted morphology method. ... 24

Figure 4.4: Comparison of the continental-scale conductivity products. 26

Figure 4.5: Density comparison of continental-scale conductivity products. 27

Figure A.1: Observed water table depth, in meters, across the High Plains. 40

Figure A.2: Modeled water table depth, in meters, across the High Plains. 42

Figure A.3: Observed distribution of water table depth, in meters, across the High Plains. 41

Figure A.4: Modeled distribution of water table depth, in meters, across the High Plains. 43

Figure B.1: Results from Luo et al 2012 compared to the preliminary results of our estimate across the High Plains. 46

Figure C.1: Parameters used to estimate hydraulic conductivity using the methodology. 47

LIST OF TABLES

Table 2.1: Parameters, symbols, and units..... 11

Table 5.1: Hydraulic conductivity (K) values at first and second peaks in the density distributions for the four hydraulic conductivity products generated.. 29

CHAPTER 1

INTRODUCTION

As the global population continues to increase, our fresh water resources face a growing demand and continue to decline (Konikow, 2015; Konikow & Kendy, 2005; Singh, 2014). Groundwater is the largest store of terrestrial freshwater, and accounts for 33% of water withdrawals globally (Famiglietti, 2014; Siebert et al., 2010). Representing terrestrial water fluxes at the continental and global scale has previously been highlighted by the hydrologic community as a pressing need (Alcamo et al., 2003; Wood et al., 2011). Because hydrologic responses to anthropogenic intervention surpass the catchment scale (Bierkens, 2015), it is imperative that we continue to improve continental and global scale hydrologic models and the data with which they are informed (Bierkens, 2015; Wada et al., 2014; Wada et al., 2010; Wood et al., 2011). If we are able to more accurately represent the behavior of water in the subsurface through large-scale integrated hydrologic models, then we will be able to better inform policy-makers and stakeholders and understand climactic influences on groundwater resources. Additionally, groundwater has been shown to be increasingly important not only for anthropogenic purpose, but also for vegetation processes such as transpiration (Maxwell & Condon, 2016) and land energy fluxes (Kollet & Maxwell, 2008; Larsen et al., 2016). Being able to better estimate regional conductivity values will directly affect our ability to model regional hydrology, land energy fluxes, and groundwater reserves.

This study estimates hydraulic conductivity over the Continental US (CONUS). I extend a method presented in Luo et al. (2012) to produce a new seamless conductivity map across the continental US at both subwatershed (HUC12) and subbasin (HUC8) resolution. I then compare this new conductivity products to other existing large-scale products. The mathematical model

used to estimate hydraulic conductivity (Luo & Pederson, 2012) will be tested for sensitivity to its parameters to lend a better understanding of its limitations. Additionally, all continental-scale products used in the calculations are accessible freely online. The resulting seamless product will then be compared to hydraulic conductivity values derived from USGS primary and secondary aquifer data and recent products from Gleeson et al. (2011, Huscroft et al., 2018) to understand the range of values that this method produces within current literature.

This study will contribute to the current body of continental scale subsurface products and provide an additional product for continental scale hydrologic modelers. This method accounts for watershed geomorphologic variability with few parameters and expunges relics of state and political boundaries. The new product will be used to inform the subsurface for new runs of the ParFlow-CLM CONUS integrated hydrologic model, which is 6.2 million square-kilometers and includes most major river basins in the US (Maxwell & Condon, 2016).

CHAPTER 2

BACKGROUND

This study estimates hydraulic conductivity across the continental US. Regional and global-scale products have previously been generated, though the body of existing of available products is limited. Below, prior studies on the regional and global influences of groundwater sustainability, subsurface characterization, and large-scale hydrologic models are discussed that highlight the need for continued improvement of continental-scale products.

2.1 Groundwater Sustainability and Demand: Regional and Global Impacts

Groundwater sustainability is a growing global issue in the face of an increasing population and freshwater demand (Scanlon et al., 2017). It has been suggested that global and regional models are insufficient in capturing total water storage anomalies because nearly all land surface models lack human intervention such as groundwater pumping and irrigation (Scanlon et al., 2018). However, the integration of groundwater into large-scale hydrologic models is already challenged by available permeability data (Gleeson et al., 2011). Irrigation accounts for 90% of global water consumption and 38% of irrigation areas are equipped with groundwater irrigation. Furthermore, the US is the third most irrigation intensive country in the world (Siebert et al., 2010). In 2012, Gleeson at al. show that we are facing widespread groundwater stress globally by comparing the groundwater footprint of principle aquifers to the current saturated area.

Groundwater stress in the High Plains and Central Valley are two examples of regional groundwater stress in the face of global pressure on our groundwater resources (Gleeson et al., 2012). The High Plains aquifer provides irrigation for approximately 20% of grain and cattle

production in the US (McGuire, 2014), and is ranked first among aquifers in the US for total groundwater extraction (Scanlon et al., 2012). The United States Geological Survey began monitoring water level depth from observational wells throughout the High Plains Aquifer (Ogallala) through a directive from Congress to report on changes in water level in the High Plains region (Water Resources Development Act of 1986). Historic and current water level data have thus been compiled from a pre-development baseline (1950-prior) to the present (McGuire, 2017). The High Plains aquifer has faced an area weighted decline of 15.8 feet since "pre-development" 1950 (USGS NE WSC, 2015). The High Plains (HP) has a consistent geographic trend in depletion rates, in that the Southern HP experiences larger depletion than the Northern HP due to its geology and storage capacity (Scanlon et al., 2012). The heterogeneous subsurface geology and spatially variable groundwater decline across the High Plains highlights the growing demand for groundwater resources in the face of a growing global population with stressed resources, and the need for more regional-scale conductivity estimates. The High Plains Aquifer, the Mississippi Embayment, and the Central Valley aquifer system account for nearly two-thirds of groundwater depletion in the US (Konikow, 2015). The Central Valley experiences a similar north-south trend in depletion as the High Plains, with the greatest water level changes in the Tulare Basin in the southern CV where precipitation is lowest and surface water deliveries are limited (Scanlon et al., 2012).

Hydraulic conductivity is often a controlling parameter for groundwater baseflow to streams, and groundwater may act as a buffer for stressed surface water flows (Hale et al., 2016). This is of particular importance in regions that face intensive water-management in which the groundwater extraction may result in decreased streamflow. One example of this is the 3,625 square-kilometer Rattlesnake Creek basin in southern Kansas. Though modelling efforts are

important to management issues, the region has limited hydraulic conductivity estimates, and existing values vary greatly among boreholes. Sophocleous et al. (1999) indicate that this is an extreme limitation for regional modeling of the basin. Additionally, groundwater depletion and loss of streamflow has also been linked to fragmenting of regional fish assemblages in regions of Colorado and Kansas, highlighting an important ecological application of regional groundwater-surface water models (Perkins et al., 2017).

While groundwater flow is a primary focus of hydrologic modeling, contaminant modeling is also of global importance to human and environmental health (Loague & Corwin, 1996). In 2010, the USGS developed both a steady-state and transient model of the 1,940 square-mile Eastern Snake River Plain Aquifer in order to evaluate the movement of waste-disposal contamination (Ackerman et al., 2010). A particle-tracking simulation revealed that the average linear velocities of contaminant dispersions predicted in the model are largely influenced by hydraulic conductivity. Hydraulic conductivity estimates from borehole measurements are noted as a hindrance in the model, citing that local scale conductivity measurements were limiting to inform a large-scale model (Ackerman et al., 2010).

2.2 Subsurface Characterization

Studying hydrology in most capacities requires knowing the hydraulic conductivity of the domain (Butler, 2005) and how spatial heterogeneity in the porous media will influence groundwater flow (Zheng & Gorelick, 2003). Permeability and hydraulic conductivity are fundamental components for analyzing groundwater fluxes (Fetter, 2001); however, the methods by which permeability and hydraulic conductivity are measured vary greatly among local, regional, and global scale measurements. Local scale measurements can be taken using slug and pump tests at individual boreholes. This will provide a value for the given point, but yield limited

information about variations in conductivity for the surrounding aquifer (Butler, 2005). The large-scale (greater than five kilometer) conductivity or permeability estimates are frequently regarded as the geometric mean of local measurements which are assumed to capture the effective conductivity of a site (Renard & de Marsily, 1997; Zinn & Harvey, 2003); however, effective conductivity values vary with scale and introduce uncertainty into aggregated representations (Dewandel et al., 2011; Gelhar et al., 1992). Though permeability and conductivity of various lithologies can be directly tested in a controlled laboratory (Cherry et al., 1975), generating large-scale estimates requires accumulating and averaging existing lithologic and hydrologic data.

Illman (2006) analyzes the spatial dependency of permeability values in an unsaturated tuff in central Arizona. They suggest that the permeability scale effect is controlled by fluid conducting fracture connections which are also dependent upon scale (Illman, 2006). Neuman (1990) present a fractal model for log-scale conductivity consistent with scale effects shown in field and lab experiments. Their study results in a scaling rule for conductivities that could be applied over a broad range of geologic mediums and scales (Neuman, 1990). The results of such studies indicated the need for conductivity and permeability estimates that correspond to the study scale, such that local measurements will not be appropriate for global studies and vice versa.

The results of Gleeson et al. (2011) provide the first look at global near-surface permeability for saturated terrestrial lithologies, stated to be appropriate for depths of 100 meters, in the Global Hydrogeology Maps (GLHYMPS). Two hundred and thirty hydrogeologic regions were derived from calibrated models and grouped into seven hydrolithologic categories (Gleeson et al., 2011). The permeability values were derived by assigning terrestrial

hydrolithologies with a geometric mean permeability for each lithology from local-scale (less than one kilometer) and regional-scale (greater than five kilometer) values previously compiled in literature. This product includes residual state boundaries, and emphasizes the lack of hydrogeological data over large scales (Maxwell & Condon, 2016).

The GLHYMPS product has been implemented into several global and regional-scale hydrologic models and land surface models, such as the Continental US configuration of the integrated hydrologic model ParFlow coupled to the land surface model CLM, CONUS 1.0 (Maxwell & Condon, 2016), and the coupled global model of the land surface model PCR-GLOWB and MODFLOW (de Graaf et al., 2014). An updated product, GLHYMPS 2.0, was published in 2018 and presents a global two-layer permeability map (Huscroft et al., 2018). This product built upon the existing GLHYMPS product by providing an improved representation of unconsolidated material at shallower and deeper depths based on recent advances in global mapping of unconsolidated material (GUM) (Börker et al., 2018) and global depth to bedrock (SoilGrids) (Shangguan et al., 2016). The results of this study provide additional permeability data at the global scale and further highlight the lack of abundant data products across scales in the hydrologic community. The GLHYMPS 2.0 product contains similar residual boundaries as GLHYMPS, and the authors further suggest a global effort to consistently re-map geologic units at higher resolution (Huscroft et al., 2018).

The GLHYMPS 2.0 dataset represents a two-layer global compilation of unconsolidated sediments and geology (Huscroft et al., 2018). This builds upon the first iteration of the global dataset (GLHYMPS) which lacked data for unconsolidated regions. The new iteration addresses this gap by the addition of the GUM (Börker et al., 2018) to the original compilation which global paired permeability data with the Global Lithological Map (GLiM) (Hartmann &

Moosdorf, 2012; Huscroft et al., 2018). The new map shows some resolution to the residual survey artifacts in the initial map, however still highlights the deficiency of consistent and abundant global geologic and hydrologic data.

Wei Luo and his colleagues present a method for estimating hydraulic conductivity in steady-state systems using surface drainage patters (Luo et al., 2010). This method is intrinsically tied to the Dupiut-Forcheimer assumptions for steady state groundwater flow, which state that groundwater flow is horizontal in an unconfined aquifer, and that the groundwater discharge is proportional to the aquifer's saturated thickness (Hantush, 1962). Their method is based on these assumptions and relates incised valley depth, saturated thickness, groundwater recharge rate, and drainage density to hydraulic conductivity. This method has been tested over the Cascades of Oregon, the Mare Tyrrhenum Quadrangle, and the High Plains with good agreement to existing borehole data (Luo et al., 2010; Luo et al., 2011; Luo & Pederson, 2012). This method is only applicable for steady state representations, without any anthropogenic intervention to surface and subsurface flows (Luo et al., 2010).

2.3 Global and Continental Hydrologic Models

Global and continental scale hydrologic models rely on input data from observation, however existing hydrogeologic data is limited (de Graaf et al., 2014; Maxwell & Condon 2016). Continental-scale models have been called an integral resource for climate forecasting and water resource planning since decades passed (Wood et al., 1997), however the uncertainties within the models would be reduced by better data availability (Abbaspour et al., 2015). Uncertainty and limitation in available hydraulic conductivity data has been noted as a limitation in regional (Ackerman et al., 2010; Sophocleous, 1999), continental (Maxwell et al., 2015), and global hydrologic models (de Graaf et al., 2014). A continental model and global model are described

below, both of which have used existing continental and global products and indicated that the development of additional large-scale products would improve these models.

ParFlow-CLM is a fully integrated hydrologic model that solves the 3-dimentional Richards equation for variably saturated subsurface flow, and the diffusive or kinematic wave equation for surface flow. It is fully coupled to the Common Land Model (CLM) to account for land surface processes and solves a full energy balance (Maxwell & Miller, 2005). The model has been configured and run over a domain that captures 6.3 million square-kilometers of the Continental US, including eight major river basins, and represents all principal components of the water energy budget at one square-kilometer lateral resolution (Maxwell & Condon, 2016). The model has been used to study many different hydrologic problems, including groundwater-surface water interactions and groundwater depletion scenarios (Condon & Maxwell, 2014; Condon & Maxwell, 2014; Gilbert et al., 2017; Maxwell & Condon, 2016). The subsurface of the ParFlow-CLM CONUS model is divided into five vertical layers of 0.1, 0.3, 0.6, 1.0 and 100 meter thicknesses, respectively. The top two meters of the CONUS domains are defined by the soil survey geographic database (SSURGO), and the lower 100 meters of the model are defined by global permeability values derived from regional hydrolithologies compiled globally (Gleeson et al., 2011). Gleeson's study focuses on quantifying regional permeability for saturated terrestrial lithologies, and defines the scale for the permeability based on the scale of data collection. This work specifically focuses on large-scale (greater than five kilometer) permeability, in order to negate any small-scale effects on permeability, such as fractures (Gleeson et al., 2011). The permeability values are modified for input to the CONUS model by changing the mean and variance (Maxwell & Condon, 2016). After the model was initialized, a one-year simulation ran using hourly NLDAS-2 historical meteorology data from water year

1985 (WY1985), which represents an average water year, to define a “pre-development” scenario (Maxwell & Condon, 2016). The model has also run with groundwater extraction, resulting in a “post-development” scenario using meteorology data from WY1985.

A 2014 study by de Graaf et al. developed a steady state ground water model and land surface model of the terrestrial world excluding Greenland and Antarctica. This study provides a look at global groundwater depths at high grid resolution (11-kilometer at the equator). The groundwater model MODFLOW was used to constrain water table depths assuming a steady-state system across the globe, and was coupled to the land surface model PCR-GLOBWB (van Beek & Bierkens, 2009). The original groundwater component in PCR-GLOBWB was replaced by a MODFLOW groundwater layer to simulate lateral groundwater flow for a single layer unconfined aquifer. Lithologic properties for the global layer were derived from the global lithologic map (GLiM) which describes 16 global lithologic classes and 26 subclasses (Hartmann & Moosdorf, 2012). Saturated permeability values were derived from GLHYMPS, previously described above (Gleeson et al., 2011). The MODFLOW groundwater layer and PCR-GLOBWB land surface layers were developed at six-degree grid resolution and coupled offline to run for a 50-year simulation period from 1960 to 2010 (de Graaf et al., 2014).

Table 2.1: Parameters, symbols, and units.

Parameter	**Symbol**	**Units**
Hydraulic Conductivity	K	L/T
Permeability	k	L^2
Recharge	R	L/T
Precipitation	P	L
Infiltration percentage	i	-
Evapotranspiration	ET	L/T
Aquifer thickness	H	L
Drainage density	D	1/L
Valley depth	d	L
Viscosity	μ	M/LT
Density	ρ	M/L^3
Gravity	g	L/T^2

CHAPTER 3

METHODS

The methods used to estimate hydraulic conductivity across the continental US using watershed geomorphology are outlined below in section 3.1. Hydraulic conductivity values were also assigned to the USGS Principle and Secondary aquifer maps, and the methods used for that evaluation are outlined in section 3.2. This method carries the Dupit-Forchheimer assumptions and Darcy assumptions for steady state, unconfined groundwater flow. Each product that was acquired for this study from other sources carries its own uncertainly which is acknowledged.

3.1 Estimating hydraulic conductivity using watershed geomorphology

This method based upon Luo et al. (2012) is used to generate a hydraulic conductivity product across the continental US. This requires the generation of four continental scale products: valley depth (d), drainage density (D), potential aquifer thickness (H), and recharge (R). Figure 3.1 presents a conceptual model of this method.

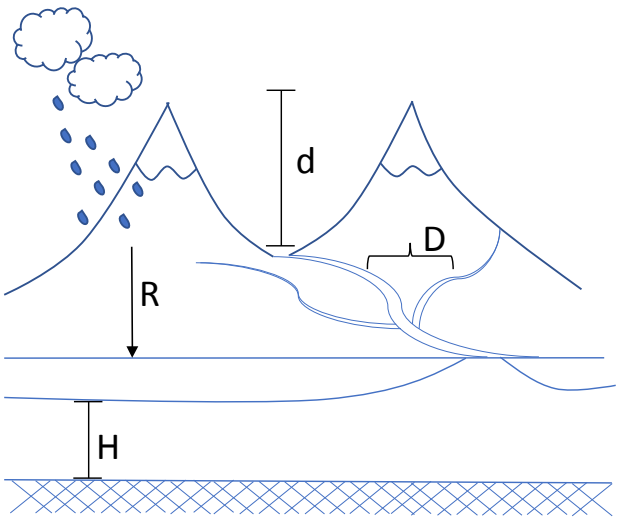

Figure 3.1: Conceptual model showing geomorphology parameters: drainage density of the watershed (D), valley depth (d), recharge (R), and aquifer thickness (H).

Each product is generated using freely available data, R, and QGIS; all parameters are estimated at both subwatershed (HUC12) and subbasin (HUC8) resolution to understand the sensitivity of the results to scale. We chose to average each parameter by subwatershed (HUC12) instead of using a local search annulus. Averaging by subwatershed (mean polygon area of 104 km^2 (Natural Resource Conservation Service, 2018)) will provide comparable resolution to the mean polygon area of North America product from Gleeson et al. (2011) (75 km^2 mean polygon area in North America) and Huscroft et al. (2018) (91.2 km^2 average polygon area for GUM units and 123 km^2 average polygon area for GLiM units), and finer resolution than the USGS Aquifer Maps (1,536 km^2 mean polygon area; United States Geological Survey, 2018d). The methods used to generate each input parameter product and to calculate hydraulic conductivity at subwatershed resolution are outlined below. A total of four hydraulic conductivity products were generated using the following methods.

3.1.1 Valley depth (d)

Valley depth (d), is estimated using the NASA Shuttle Radar Topographic Mission (SRTM) 90-meter resolution digital elevation model (DEM) from CGIAR Consortium for Spatial Information. In order to derive valley depth (d) from the DEM raster product, the product was first clipped to the extent of the continental US, and overlain with a subwatershed shapefile with the USGS Watershed Boundary Dataset (WBD; Natural Resource Conservation Service, 2018). The zonal statistics tool in QGIS is then used to find the maximum and minimum elevation within each subwatershed polygon. The results from zonal statistics are automatically joined to the subwatershed shapefile. The valley depth for each subwatershed is found by subtracting the minimum elevation from the maximum elevation, therefore producing a maximum depth of incision in each subwatershed.

3.1.2 Drainage density (D)

Drainage density (D) is generated using the USGS National Hydrography Dataset (NHD) which contains delineated streams across the entire continental US (United States Geological Survey, 2018a). This product contains other water features including culverts, drainage pipes, and lakes; however, only the streams were used since the other hydraulic structures are not present in the CONUS model and would result in a disingenuous representation of drainage features. Due to the size of the USGS NHD delineated stream file, R and QGIS were unable to store the complete continental dataset. Because of this limitation, the streams were clipped by HUC2 regions to generate 18 smaller stream files, and the HUC12 WBD was also clipped by HUC2. The stream lengths were summed by subwatershed per HUC 2 region, generating 18 separate stream density files. This was done using the "Sum line lengths" vector analysis tool in QGIS. The stream length polyline layer is used as the "Lines" input, and the watershed polygon layer as the "Polygon" input. Next, the drainage density is calculated by dividing the sum of stream lengths in each watershed by the area of the subwatershed, both in meters. The stream density was found for each subwatershed in each HUC2 region, and then all 18 regions were merged back together into one continuous product at subwatershed resolution.

3.1.3 Aquifer thickness (H)

Aquifer thickness (H) for each subwatershed was estimated using a 250-meter resolution global depth to bedrock product (Shangguan et al., 2016) which represents modeled depth of soils and regolith. Their model used 661,441 borehole observations, DEM-based hydrologic and morphologic parameters, MODIS surface and vegetation products, and lithologic units to estimate depth to bedrock. Their final product contains estimations at 250-meter resolution, and was checked against 661,441 borehole logs in the United States. This product is freely available

as a raster layer through SoilGrids (Hengl et al., 2017). To generate mean aquifer thickness, the raster was downloaded and overlain with the subwatershed shapefile, and the zonal statistics tool is used to calculate the mean depth to bedrock in each subwatershed polygon. The mean depth to bedrock was assumed to represent the maximum potential thickness where unconfined aquifers remain saturated.

3.1.4 Recharge (R)

Recharge (R) is estimated using two different methods to better understand the sensitivity of the Equation 3.1 to the recharge parameter. The first method follows the conceptual model explained in Luo et al., 2012 which states that recharge in an unconfined aquifer is equal to the precipitation rate times the soil infiltration percentage:

$$R = P\ x\ i \tag{3.1}$$

The soil infiltration percentage product (i) was developed using soil hydrologic spatial products from the Natural Resources Conservation Service STATSGO data base (Schwarz & Alexander, 1995). The soil products include hydrologic group information of each soil type, defined by a decimal value from 0.0 to 4.0. Values closer to zero indicate a sandier soil, and values closer to four indicate soils with a higher abundance of clay-rich minerals. These products are available for download from the Web Soil Survey in shapefile format for each HUC2 region. All 18 HUC2 polygons were downloaded and merged to generate a continuous product. The mean hydrologic type within each subwatershed is found by using the spatial query tool in QGIS. The mean hydrologic type is then matched with an infiltration percentage defined in a prior USGS geohydrology publication (Gutentag et al., 1984) by exporting the data in R and using a for-loop to assign the appropriate percentage to each subwatershed. This results in a shapefile that has the mean infiltration percentage, *i*, for each subwatershed. The precipitation rate for each

subwatershed is derived from the PRISM 30-year annual average product available for download from the Oregon State Climate Group (PRISM Climate Group, 2018). The 30-Year Normal raster was overlain with the subwatershed shapefile. Zonal statistics were run to find the mean precipitation for each watershed. The final recharge product was made by joining the subwatershed mean precipitation shapefile to the watershed mean infiltration, then multiplying the mean precipitation for each watershed by the corresponding infiltration percentage for that watershed. This yields a value that represents the total recharge.

The second way that Recharge (R) is estimated is by using a conceptual model that states that recharge to a steady-state unconfined aquifer is equal to precipitation minus evapotranspiration:

$$R = P - ET \tag{3.2}$$

A continental scale evapotranspiration product from the USGS is used (Sanford & Selnick, 2013). This product was generated by the USGS using observed ET values from 838 real-time gaged watersheds across the US with complete flow records from 1971 to 2000. The product's evapotranspiration rates represent empirical estimates derived from a regression equation and are constrained by water balance data from the gage stations. The ET rates are representative of an average rate from 2000 to 2013. Zonal statistics were used to estimate the mean ET rate in each subwatershed. In subwatersheds where the ET rate is zero or negative, such as in the southwestern desert, a minimum rate of 10^{-3} meters per year is applied to prevent large areas of the western US of zeros or negative conductivity values. The 30-year average precipitation product from the PRISM climate group is used as the precipitation product. Next, the subwatershed average evapotranspiration shapefile was joined to the precipitation shapefile,

and the ET rate was subtracted from the precipitation rate using the field calculator to find the average recharge rate of each subwatershed.

3.1.5 Hydraulic Conductivity (K)

The watershed averaged parameters were used to solve for hydraulic conductivity (K), in units of m/s, using the equation presented by Luo et al. (2012):

$$K = \frac{R}{D^2[H^2 - (H-d)^2]} \tag{3.3}$$

This relationship is based upon Darcy's law, which states that groundwater flow is proportional to hydraulic conductivity, cross-sectional area, and head gradient:

$$Q = -KA\frac{dh}{dl} \tag{3.4}$$

Equation 3.1 is also based upon the Dupuit equation, developed in 1863, for steady flow in an unconfined aquifer (Fetter, 2001). This equation states that the flow per unit width is related to the hydraulic gradient and the hydraulic conductivity of the aquifer.

$$q' = \frac{1}{2}K\left(\frac{h_1^2 - h_2^2}{L}\right) \tag{3.5}$$

Hydraulic conductivity (K) is the coefficient of permeability (k), and the relationship between the two is represented in Equation 3.4. All products in this paper will be presented in terms of hydraulic conductivity.

$$k = K\left(\frac{\mu}{\rho g}\right) \tag{3.6}$$

The final product using this method carries the assumptions that the aquifer is unconfined, saturated, and effectively drained. We evaluated Equation 3.3 to understand the

relationship between hydraulic conductivity and each of its parameters by varying one parameter at a time while holding the others constant at an average value. The sensitivity of this equation is discussed in Luo et al. 2010; however, we wanted to test all parameters in this equation at once. Perturbing the parameters one at a time shows that recharge (R) and hydraulic conductivity (K) have a positive linear relationship, so as recharge increases by 1 [L/T], K will increase by 1.6E-4 [L/T] if all other values are held at their average. As R changes by one order of magnitude, K will also change by one order of magnitude. This indicates that variations in the recharge parameter have a linear impact on K and thus K is sensitive to any variation in R. K and drainage density (D) have a negative exponential relationship when D is below 0.1, and there is no change in K when D is above 0.1. This relationship means that in areas with low topography, K will have a high sensitivity to stream features. We can also see that aquifer thickness (H) and valley depth (d) both have a root-power relationship to K. This means that when H is half of d, K goes to infinity, and when H is less than one half of d, K is negative. These relationships are in agreement with those discussed in (Luo et al., 2010). The inverse of this relationship exists when examining the relationship between K and d. When d is more than twice H, K is negative, and when d is twice H, K goes to infinity. The relationships seen in this analysis are mathematically intuitive, given the range of values for each parameter, whether or not they are in the denominator or numerator of the equation. Figure 3.2 may serve as a guideline for input parameter constraints.

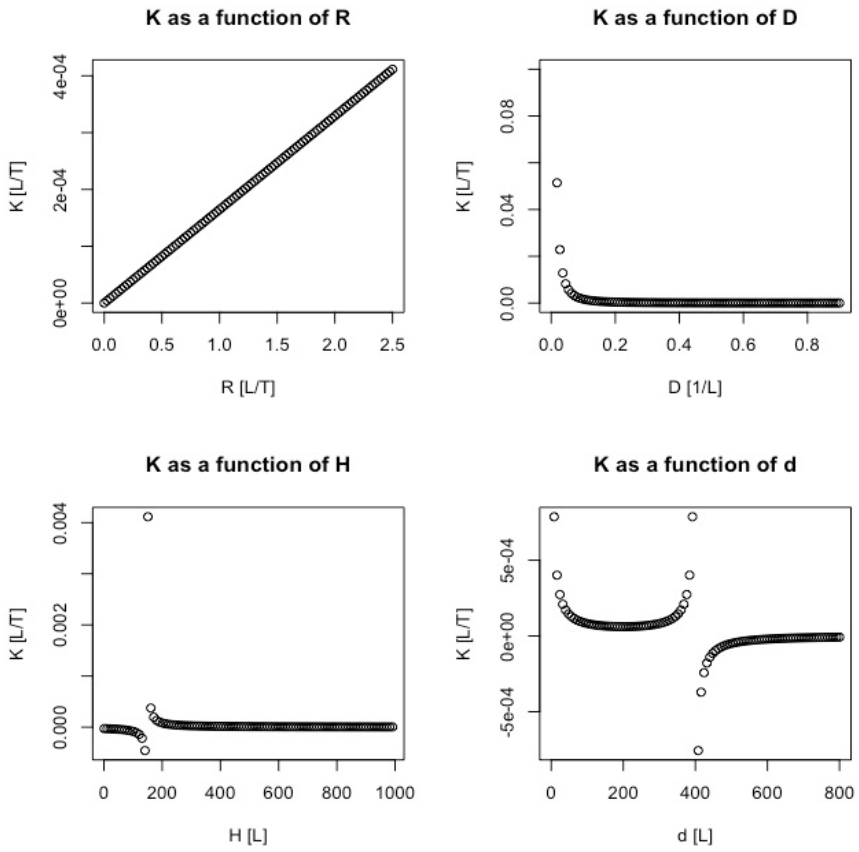

Figure 3.2: The relationship between K and each of its parameters using Equation 3.3.

3.2 USGS Primary Aquifers and Secondary Hydrogeologic Regions

The USGS has compiled lithologic data for 62 principle aquifers in the US. This data is available in several spatial formats via the USGS groundwater information website (United States Geological Survey, 2018c). The regions outside of the principle aquifers were left as "other rock," and account for about 40% of the continental US. Recently, these "other rock" regions were evaluated for geological similarities among the regions and defined as 69 secondary hydrogeologic regions (SHRs) (Belitz et al., 2018). The principal aquifers (PAs) and secondary hydrogeologic regions (SHRs) polygons were downloaded and spatially joined to generate complete coverage of the continental US. Each dataset contains geologic information for the

principle or secondary hydrologic regions. The geologic information in the joined PA-SHR shapefile evaluated and nine unique geologic types were identified: unconsolidated sand and gravel, semi-consolidated sand, sedimentary, sandstone, carbonate, crystalline, volcanic, igneous and metamorphic, and mixed. This information was used to match each geologic type with a corresponding hydraulic conductivity value taken from Heath, 1983. The geologic data was exported to R and a for-loop was used to assign a K value to each hydrogeologic type. Once each hydrogeologic type is assigned a value, the mean hydraulic conductivity for each subwatershed is found by performing a spatial query in QGIS. This generates a hydraulic conductivity product with values representative of principle and secondary aquifer geology at subwatershed resolution.

CHAPTER 4

RESULTS

The results of the adapted morphology method are described below in section 4.1. Four iterations were run across the continental US to understand the influence of recharge and scale on this method. The results of the USGS PA-SHR analysis and a comparison of the morphology results to other continental-scale products, including the PA-SHR product, are in section 4.2.

4.1 Morphology Method Results

The adapted morphology method was first tested across the High Plains Aquifer to assess its reproducibility in comparison to Luo et al. (2012). The results of the test across the High Plains show good agreement with those presented in Luo et al. (2012). Methods and results for this test can be found in Appendix B. Next the methodology was used to evaluate all four variables (R, d, D, and H) across the continental US using R and QGIS. The kernel density estimates for each parameter used to calculate K across the continental US is shown in Figure 4.1. The spatial distribution of each parameter can be seen in Appendix C.

Recharge exhibits bimodality at both subwatershed (HUC12) and subbasin (HUC8) resolution. The PME estimates show a broader range of values than the PI estimates at both resolutions. Drainage density shows bimodality at subwatershed resolution, and upscaling to subbasin appears to smooth out this behavior. Aquifer thickness appears to have no sensitivity to resolution. Valley depth shows a broader range of estimates at subbasin resolution.

In instances when the rate of evapotranspiration exceeded the rate of precipitation, a minimum recharge value was assigned to avoid a negative or zero recharge. This is because Equation 3.3 disallows negative or zero recharge. The mean recharge value derived by Equation 3.1 (precipitation times infiltration percent) was 7.4 cm/yr. This is within the same order of

magnitude as the mean recharge value from Luo et al., 2012, which was 3.6 cm/yr derived using a similar method; however, their mean recharge value only reflects the High Plains aquifer. The mean recharge calculated in the first test across the High Plains was 5.5 cm/yr. Both of the mean values from the method used in this study are within the same order of magnitude, but higher on average.

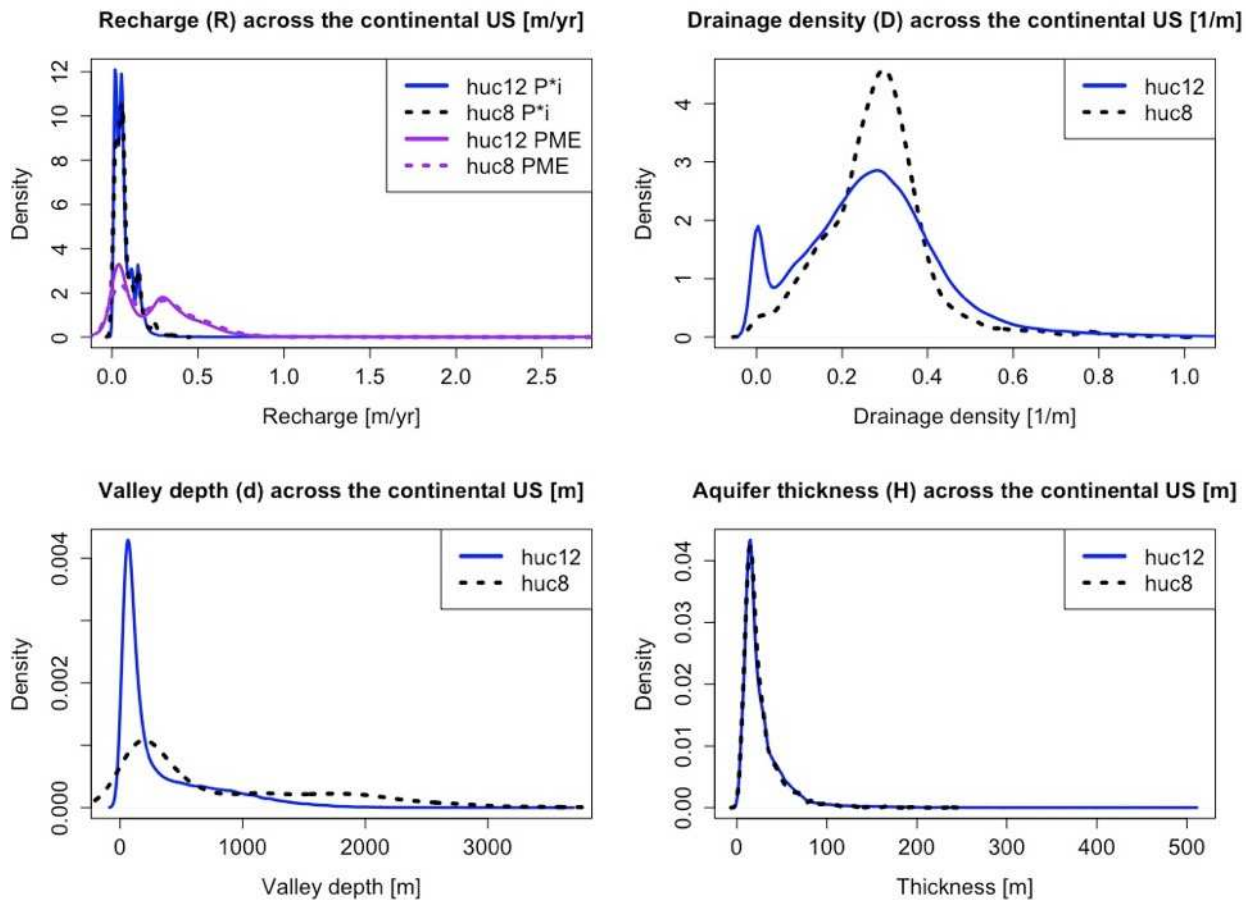

Figure 4.1: Density distribution of all variables used to calculate hydraulic conductivity.

Next, Equation 3.3 was used to generate four hydraulic conductivity products across the continental US: K estimated at HUC12 resolution with recharge modeled as precipitation times infiltration percentage (HUC12 PI); K estimated at HUC12 resolution with recharge modeled as precipitation minus evapotranspiration (HUC12 PME); K estimated at HUC8 resolution with

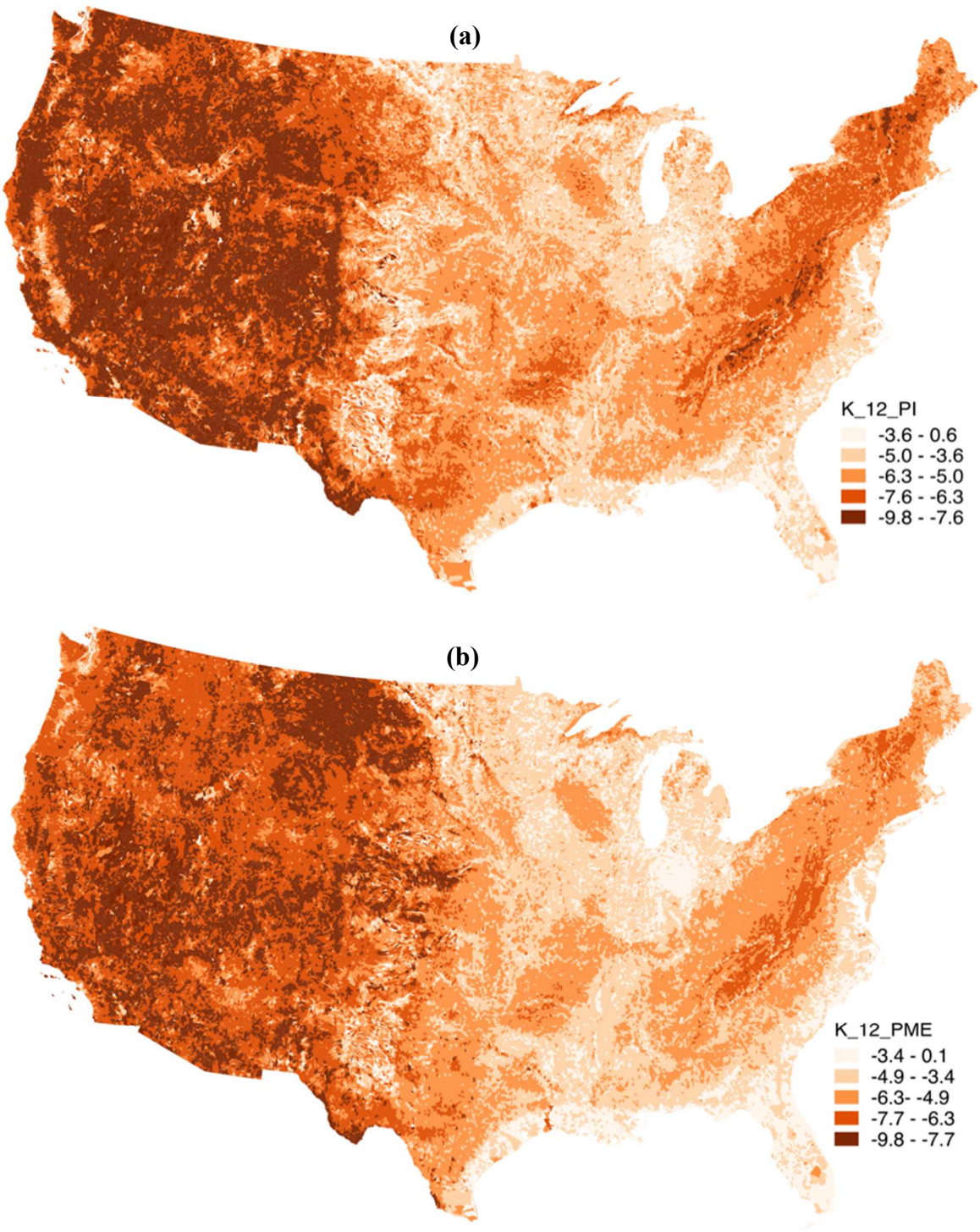

Figure 4.2: Hydraulic conductivity (K) values [m/s] estimated using the adapted morphology method (Equation 3.1), at subwatershed (HUC12) resolution; (a) K estimated using precipitation times infiltration percent as recharge (R); (b) K estimated using precipitation minus evapotranspiration as recharge (R).

recharge modeled as precipitation times infiltration percentage (HUC8 PI); and K estimated at HUC8 resolution with recharge modeled as precipitation minus evapotranspiration (HUC8 PME). The resulting products from the HUC12 analyses can been seen in Figure 4.2. The hydraulic conductivity estimates in each of the four products are within a similar range, from 10^{0} to 10^{-10} m/s. The products estimated using precipitation minus evapotranspiration as the recharge parameter show higher values by about one order of magnitude (Figure 4.3, Table 5.1). All products exhibit bimodal behavior, as seen in Figure 4.3.

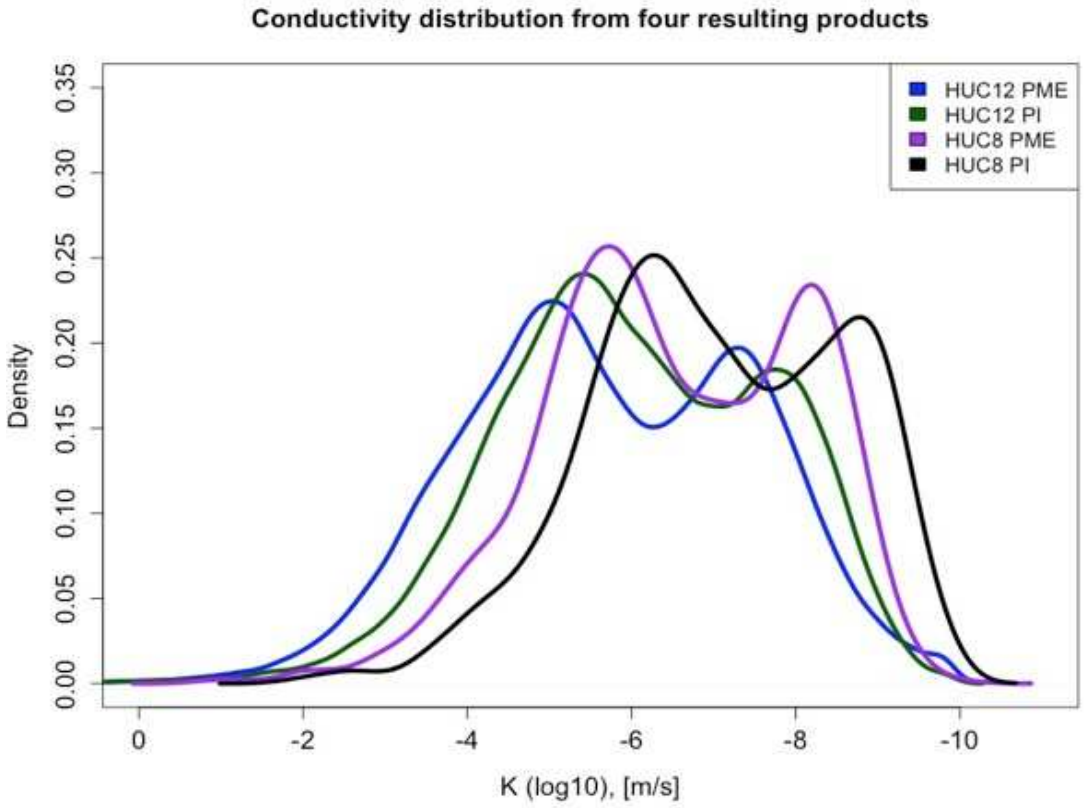

Figure 4.3: Results of the four different K estimates using the adapted morphology method.

Equation 3.3 was unable to predict values for 6.4% of the total 83,228 HUC12s in the continental US due to mathematical constraints in the equation. A nearest neighbor interpolation

was used to assign values to the subwatersheds that have parameters incompatible with the morphology equation (Equation 3.3). The parameter values for each HUC8 subbasin were within the bounds of the mathematical constraints and a conductivity value was able to be calculated for subbasin.

4.2 Comparison of Datasets

The product generated from the USGS Primary and Secondary hydrogeology regions (hereafter referred to as USGS PA-SHR) and from the morphology method both exhibit bimodal behavior in conductivity values (Figure 4.4, 4.5). This is representative of the hydraulic properties of the nine geologies assigned to the primary and secondary aquifer regions. Hydraulic conductivity values were based upon literature values for each lithology (Heath, 1983) and range from 10^{-2} to 10^{-9} m/s. The boundaries in the product represent principle aquifers and secondary hydrogeologic regions.

The HUC12 PI product was compared to the GLHYMPS 2.0 map, CONUS 1.0 subsurface, and the USGS PA-SHR hydraulic conductivity map that was also generated in the study (Figure 4.4, 4.5). To facilitate model comparison, the GLHYMPS 2.0 map, the USGS PA-SHR map, and the HUC12 PI map were clipped to the extent of the 6.2 million km^2 CONUS domain and scaled to subwatershed resolution. The range of values produced from the morphology method is consistent with the GLHYMPS 2.0, CONUS, and USGS PA-SHR products across the extent of the CONUS domain, but the range of values form the CONUS subsurface parameter set has a considerably smaller range (Figure 5). Though the distribution of values is comparable (Figure 4.5), the spatial distribution of values varies among the four methods (Figure 4.4).

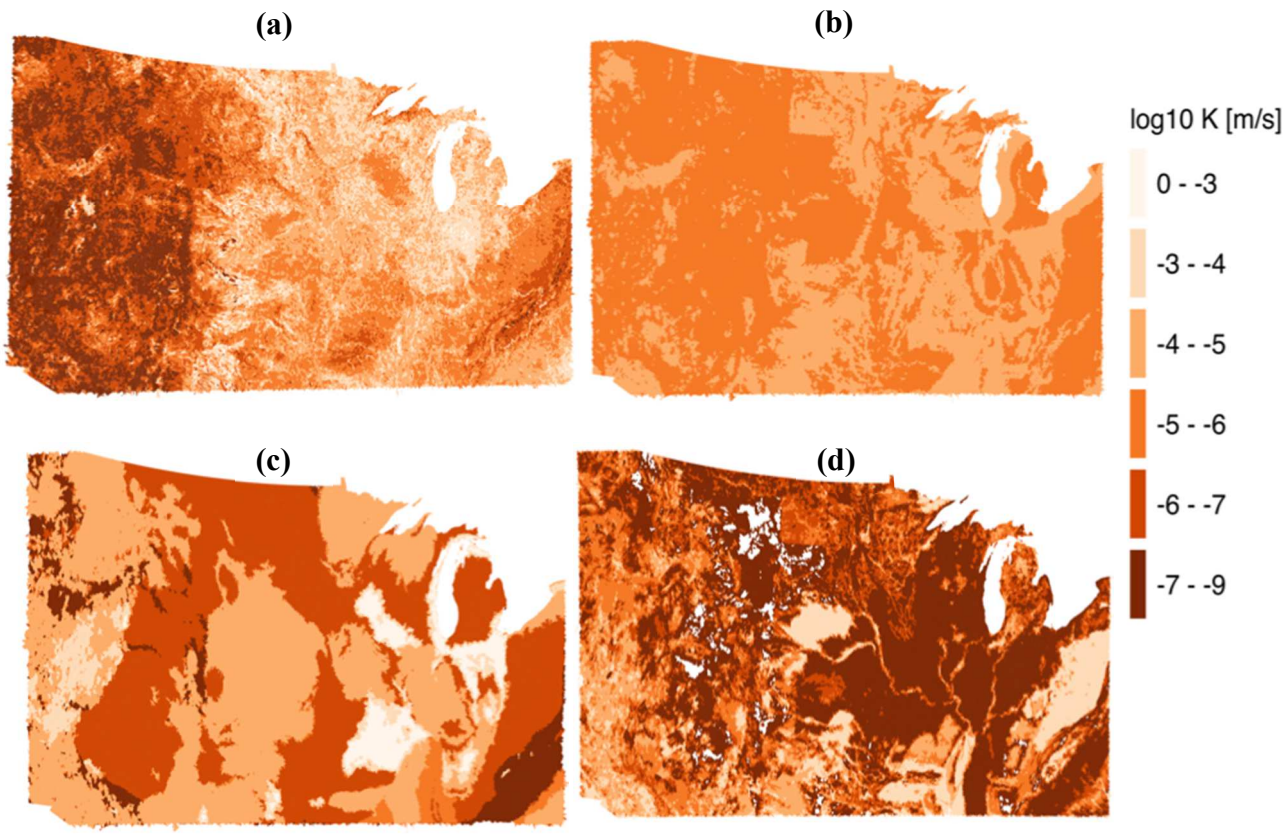

Figure 4.4: Comparison of the (a) HUC12 PI product to (b) the CONUS 1.0 subsurface, (c) USGS PA-SHR aquifer map, and (d) GLHYMPS 2.0 map, all subset over the CONUS 1.0 domain.

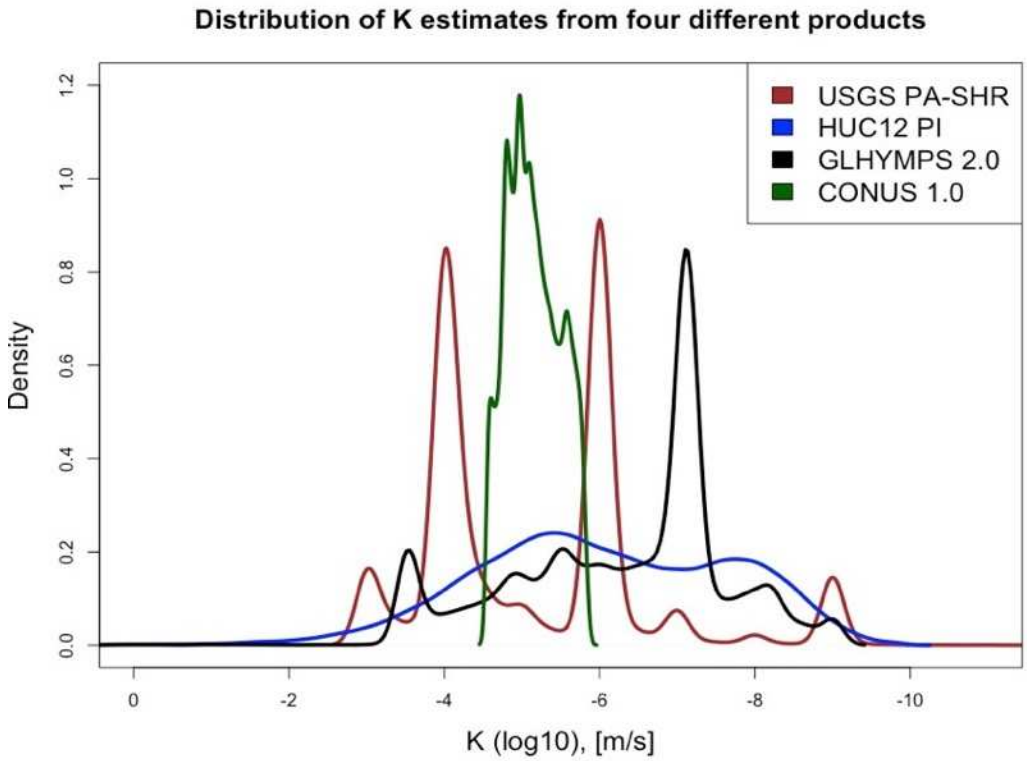

Figure 4.5: Comparison of our K product (HUC12 PI) to other continental-scale products: USGS PA-SHR, GLHYMPS 2.0, and the CONUS 1.0 subsurface.

CHAPTER 5

DISCUSSION

A novel technique is presented for generating a continental scale hydraulic conductivity product based on subbasin or subwatershed morphology. This method is based upon a method previous derived and tested in the Oregon Cascades, High Plains, and Mars by Luo et al. (2010, 2011; Luo & Pederson, 2012). In Figure 5, the HUC12 PI product is compared to the three other continental scale products. The values generated by the morphology method (Figure 5) vary across ten orders of magnitude and are within a similar distribution to the GLHYMPS 2.0, CONUS 1.0 subsurface, and USGS PA-SHR maps (Figure 5, Figure 6). Additionally, the distribution of values estimated from the morphology method are in agreement with the range of values from prior studies that used morphology to derive K (Luo et al., 2010, 2011; Luo & Pederson, 2012) as can been seen in Appendix B. The morphology product (HUC12 PI) shows lower bimodal peaks than the USGS PA-SHR map and a lower peak than either GLHYMPS 2018 or CONUS 1.0 subsurface (Figure 4.5). This suggests that this technique captures a higher degree of spatial heterogeneity and that it is able to estimate more heterogeneous conductivity values than the methods used to generate the other continental-scale products.

Though the density distribution of hydraulic conductivity values shows agreement among the four continental-scale products (Figure 4.4), the spatial distribution of hydraulic conductivity values varies (Figure 4.5). This is representative of the methodology used the derive each product, and suggests inconsistencies among methods used to collect regional data and generate large-scale products. This highlights the importance of continuing to improve regional, continental, and global scale hydrologic methods. The morphology product (Figure 4.2, Figure 4.4a) shows bimodal behavior, and a trend is apparent from East to West. Both the density and

spatial distribution of values is representative of the recharge parameter. The USGS PA-SHR maps shows a bimodal distribution (Figure 4.5), and spatial distribution of values based upon principal aquifer and secondary hydrogeologic region lithologies (Figure 4.4).

The variation in recharge values derived in this study shows the sensitivity of hydraulic conductivity to recharge using the morphology method. The values increased on average by nearly half an order of magnitude by using the "PME" recharge layer instead of the "PI" layer. This pattern was seen in all four K products that were generated in this study (Table 5.1). This is likely because recharge is the only parameter in the numerator of the hydraulic conductivity equation (Equation 3.3). As seen in Figure 3.1, hydraulic conductivity and recharge have a positive linear relationship, and as recharge increases by 1 [L/T], hydraulic conductivity will increase by 1.6E-4 [L/T].

Table 5.1: Hydraulic conductivity (K) values, in units of m/s, at first and second peaks in density distributions for each of the four hydraulic conductivity products generated and the products used for comparison. The geometric mean K values for each product are also presented. Morphology products were named according to their resolution ("HUC12" or "HUC8), methods used to estimate recharge for each (precipitation minus evapotranspiration "PME", or precipitation times infiltration percentage "PI").

Product	**K Value at First Peak**	**K Value at Second Peak**	**Geometric Mean K**
HUC12 PI	$10^{-4.83}$	$10^{-7.79}$	$10^{-5.76}$
HUC12 PME	$10^{-4.56}$	$10^{-7.12}$	$10^{-5.41}$
HUC8 PI	$10^{-6.13}$	$10^{-9.34}$	$10^{-6.84}$
HUC8 PME	$10^{-5.67}$	$10^{-8.00}$	$10^{-6.29}$
USGS PA-SHR	$10^{-4.00}$	$10^{-6.00}$	$10^{-4.98}$
CONUS 1.0	$10^{-4.97}$	-	$10^{-5.14}$
GLHYMPS 2.0	$10^{-3.76}$	$10^{-7.10}$	$10^{-6.07}$

The geometric mean conductivity values of each product are shown in Table 5.1. The values vary across two orders of magnitude, however there is agreement among products. However, the spatial dissimilarity among conductivity products highlights the variation in

methodology and datasets used to generate each product (Figure 4.4). The HUC8 PI product has the lowest geometric mean value. This demonstrates the effect of the recharge parameter on the methodology, and lose of heterogeneity due to downscaling from HUC12 to HUC8. The conductivity values for the first and second peak densities for each of the products are also included in Table 5.1. The location of density peaks demonstrates how upscaling the parameters in the morphology method influenced the range of values (Figure 4.3, Table 5.1). Averaging the recharge (R), aquifer thickness (H), valley depth (d), and stream density (D) subbasin (HUC8) lowers the K values compared to the subwatershed (HUC12) K values. Downscaling from HUC12 to HUC8 loses some spatial heterogeneity in all input parameters. Additionally, downscaling the soil infiltration percentage and PME influences the hydraulic conductivity, with recharge as an individual factor. Changing the recharge product from PI to PME influence the first and second density peak by nearly two orders of magnitude (Table 5.1). The combined effect of changing the recharge parameter and downscaling has the most pronounced influence on the density distribution among the four scenarios tested, as seen in Table 5.1 and Figure 4.3.

The HUC12 PI product values are of a similar range compared to the other three morphology products (Figure 4.5, Table 5.1), and compares well to the distribution of values from the other continental-scale products. Additionally, the geometric mean conductivity values agree among products. However, the spatial distribution among the products varies (Figure 4.4). This suggests continued improvement to methodology for collecting conductivity data at local scales and for making regional scale conductivity estimates. The mean polygon area of each subwatershed is comparable to the mean polygon area of the GLHYMPS and GLHYMPS 2.0 maps. Additionally, Luo et al. (2012) generate recharge using infiltration percentage times precipitation rate, which is how recharge was modeled for the HUC12 PI product. Therefore, the

HUC12 PI product is the most comparable to the original method (Luo et al., 2012) and is comparable to the distribution of values in other continental scale products.

Using a nearest neighbor interpolation to resolve discontinuous areas introduces some additional uncertainty into the final product, though it does provide an estimate for those watersheds based upon the method used here. Uncertainty is also present from the products that were used here to generate each parameter. Equation 3.3 was able to calculate a value for all HUC8 watersheds. This is likely due to smoothing of subwatershed heterogeneities which may reduce the chance that a combination values will align with a mathematical constraint.

CHAPTER 6

CONCLUSIONS

Using freely available inputs, a novel method was used to estimate hydraulic conductivity across the continental US. Hydraulic conductivity products were generated at subwatershed and subbasin resolution, and with two different recharge products. Results of the study demonstrated the sensitivity of the model to the recharge parameter, and how downscaling all parameters lowers the average values within the product by diminishing the spatial heterogeneity. The boundaries shown in the new product are indicative of subwatersheds, instead of arbitrary state or federal survey boundaries such as in the GLHYMPS and GLHYMPS 2.0 maps.

The hydraulic conductivity values in the morphology products fall within the average range of values in GLHYMPS 2.0, CONUS 1.0 subsurface, and the USGS PA-SHR map. The morphology products show less bimodality than the other continental-scale products, though still presents a distinctive East-West trend. This implies that the method captures more heterogeneity in conductivity values, which would lower the density peaks. The HUC12 PI product shows good agreement with GLHYMPS 2.0, CONUS 1.0 subsurface, and the USGS PA-SHR map, has a mean polygon area similar to the GLHYMPS maps, and uses a recharge product generated with a similar method presented in Luo et al. (2012). Therefor the HUC12 PI is the most successful product generated out of the four iterations.

The methodology contains steady-state assumptions and mathematical constraints (Figure 3.1), though is able to estimate hydraulic conductivity values across the majority of the US that are comparable to other continental-scale products. Though the distribution of values is similar, the spatial discrepancies suggest continued efforts to improve methods for estimating hydraulic conductivity of both the regional and local scales. The generated product will benefit the

continental-scale modeling community by providing new large-scale conductivity estimates for the US, and presenting a method that can be used in any region to calculate hydraulic conductivity using freely available data and software. This dataset is vital for the hydrologic community, a field that is inherently data-limited due to the difficulty of collecting observational subsurface data.

REFERENCES

Abbaspour, K. C., Rouholahnejad, E., Vaghefi, S., Srinivasan, R., Yang, H., & Kløve, B. (2015). A continental-scale hydrology and water quality model for Europe: Calibration and uncertainty of a high-resolution large-scale SWAT model. *Journal of Hydrology*, *524*, 733–752. https://doi.org/10.1016/j.jhydrol.2015.03.027

Ackerman, D. J., Rousseau, J. P., Rattray, G. W., & Fisher, J. C. (2010). Steady-State and Transient Models of Groundwater Flow and Advective Transport, Eastern Snake River Plain Aquifer, Idaho National Laboratory and Vicinity, Idaho, 220. https://doi.org/5123

Alcamo, J., Döll, P., Henrichs, T., Kaspar, F., Lehner, B., Rösch, T., & Siebert, S. (2003). Development and testing of the WaterGAP 2 global model of water use and availability. *Hydrological Sciences Journal*, *48*(3), 317–338. https://doi.org/10.1623/hysj.48.3.317.45290

Belitz, K., Watson, E., Johnson, T. D., & Sharpe, J. (2018). Secondary Hydrogeologic Regions of the Conterminous United States. *Groundwater*. https://doi.org/10.1111/gwat.12806

Bierkens, M. F. P. (2015). Global hydrology 2015: State, trends, and directions. *Water Resources Research*, 6682–6698. https://doi.org/10.1002/2015WR017173.Received

Börker, J., Hartmann, J., Amann, T., & Romero-Mujalli, G. (2018). Terrestrial Sediments of the Earth: Development of a Global Unconsolidated Sediments Map Database (GUM). *Geochemistry, Geophysics, Geosystems*, 997–1024. https://doi.org/10.1002/2017GC007273

Butler, J. J. (2005). *Hydrogeological methods for estimation of spatial variations in hydraulic conductivity. In Hydrogeophysics*. (Dordrecht, Ed.). Springer.

Cherry, J. A., Gilham, R. W., & Pickens, J. F. (1975). Contaminant Hydrogeology-Part 1: Physical Processes. Geoscience Canada 2(2).

Condon, L. E., & Maxwell, R. M. (2014). Groundwater-fed irrigation impacts spatially distributed temporal scaling behavior of the natural system: A spatio-temporal framework for understanding water management impacts. *Environmental Research Letters*, *9*(3). https://doi.org/10.1088/1748-9326/9/3/034009

Condon, L., & Maxwell, R. (2014). Feedbacks between managed irrigation and water availability: Diagnosing temporal and spatial patterns using an integrated hydrologic model. *Water Resources Research*, 2600–2616. https://doi.org/10.1002/2013WR014868.Received

de Graaf, I. E. M., Sutanudjaja, E. H., Van Beek, L. P. H., & Bierkens, M. F. P. (2014). A high resolution global scale groundwater model. *Hydrology and Earth System Sciences Discussions*, *11*, 5217–5250.

Dewandel, B., Maréchal, J. C., Bour, O., Ladouche, B., Ahmed, S., Chandra, S., & Pauwels, H. (2011). Upscaling and regionalizing hydraulic conductivity and effective porosity at watershed scale in deeply weathered crystalline aquifers. *Journal of Hydrology*, *416–417*, 83–97. https://doi.org/10.1016/j.jhydrol.2011.11.038

Famiglietti, J. S. (2014). The global groundwater crisis. *Nature Climate Change*, *4*(11), 945–948. https://doi.org/10.1038/nclimate2425

Fetter, C. W. (2001). *Applied Hydrogeology* (4th ed.). Pearson.

Gelhar, L. W., Welty, C., & Rehfeldt, K. R. (1992). A Critical Review of Data on Field-Scale Dispersion in Aquifers based on fractal concepts. *Water Resour. Res.*, *28*(7), 1955–1974.

Gilbert, J. M., Maxwell, R. M., & Gochis, D. J. (2017). Effects of Water-Table Configuration on the Planetary Boundary Layer over the San Joaquin River Watershed, California. *Journal of Hydrometeorology*, *18*(5), 1471–1488. https://doi.org/10.1175/JHM-D-16-0134.1

Gleeson, T., Alley, W. M., Allen, D. M., Sophocleous, M. A., Zhou, Y., Taniguchi, M., & Vandersteen, J. (2012). Towards sustainable groundwater use: Setting long-term goals, backcasting, and managing adaptively. *Ground Water*, *50*(1), 19–26. https://doi.org/10.1111/j.1745-6584.2011.00825.x

Gleeson, T., Smith, L., Moosdorf, N., Hartmann, J., Dürr, H. H., Manning, A. H., … Jellinek, A. M. (2011). Mapping permeability over the surface of the Earth. *Geophysical Research Letters*, *38*(2), 1–6. https://doi.org/10.1029/2010GL045565

Gutentag, E. D., Heimes, F. J., Krothe, N. C., Luckey, R. R., & Weeks, J. B. (1984). Geohydrology of the High Plains Aquifer In Parts of Colorado , Kansas , Nebraska , New Mexico , Oklahoma , South Dakota , Texas , and Wyoming. *U.S. Geological Survey Professional Paper*, (1400–B).

Hale, V. C., McDonnell, J. J., Stewart, M. K., Solomon, D. K., Doolitte, J., Ice, G. G., & Pack, R. T. (2016). Effect of bedrock permeability on stream base flow mean transit time scaling relationships: 2. Process study of storage and release. *Water Resources Research*, *52*(2), 1375–1397. https://doi.org/10.1002/2015WR017660

Hantush, M. S. (1962). On the Validity of the Dupuit-Forchheimer Well-Discharge Formula. *Journal of Geophysical Research*, *67*(6), 2417–2420.

Hartmann, J., & Moosdorf, N. (2012). The new global lithological map database GLiM: A representation of rock properties at the Earth surface, *13*(12), 1–37. https://doi.org/10.1029/2012GC004370

Heath, R. C. (1983). Basic Groundwater Hydrology. *U.S. Geological Survey Water-Supply Paper*.

Hengl, T., Mendes de Jesus, J., Heuvelink, G. B. M., Ruiperez Gonzalez, M., Kilibarda, M., Blagotić, A., … Kempen, B. (2017). SoilGrids250m: Global gridded soil information based on machine learning. *PLOS ONE*, *12*(2), e0169748. https://doi.org/10.1371/journal.pone.0169748

Huscroft, Jordan; Gleeson, Tom; Hartmann, Jens; Börker, J. (2018). Compiling and Mapping Global Permeability of the Unconsilidated and Consolidated Earth: GLobal HYdrologeology MaPS 2.0 (GLHYMPS 2.0). *Geophysical Research Letters*, (2017), 1897–1904. https://doi.org/10.1002/2017GL075860

Illman, W. A. (2006). Strong field evidence of directional permeability scale effect in fractured rock. *Journal of Hydrology*, *319*(1–4), 227–236. https://doi.org/10.1016/j.jhydrol.2005.06.032

Jarvis, A., Reuter, H. I., Nelson, A., & Guevara, E. (2008). Hole-filled STRM for a globe Version 4, Available from the CIGAR-CSI STRM 90m Database. Retrieved from http://strm.csi.cgiar.org

Kollet, S. J., & Maxwell, R. M. (2008). Capturing the influence of groundwater dynamics on land surface processes using an integrated, distributed watershed model. *Water Resources Research*, *44*(2), 1–18. https://doi.org/10.1029/2007WR006004

Konikow, L. F. (2015). Long-Term Groundwater Depletion in the United States, *53*(1), 2–9. https://doi.org/10.1111/gwat.12306

Konikow, L. F., & Kendy, E. (2005). Groundwater depletion: A global problem. *Hydrogeology Journal*, *13*(1), 317–320. https://doi.org/10.1007/s10040-004-0411-8

Larsen, M. A. D., Rasmussen, S. H., Drews, M., Butts, M. B., Christensen, J. H., & Refsgaard, J. C. (2016). Assessing the influence of groundwater and land surface scheme in the modelling of land surface–atmosphere feedbacks over the FIFE area in Kansas, USA. *Environmental Earth Sciences*, *75*(2), 1–13. https://doi.org/10.1007/s12665-015-4919-0

Loague, K., & Corwin, D. L. (1996). *Uncertainty in Regional-Scale Assessments of Non-Point Source Pollutants*.

Luo, W., Grudzinski, B. P., & Pederson, D. (2010). Estimating hydraulic conductivity from drainage patterns-a case study in the Oregon Cascades. *Geology*, *38*(4), 335–338. https://doi.org/10.1130/G30816.1

Luo, W., Grudzinski, B., & Pederson, D. (2011). Estimating hydraulic conductivity for the Martian subsurface based on drainage patterns - A case study in the Mare Tyrrhenum Quadrangle. *Geomorphology*, *125*(3), 414–420. https://doi.org/10.1016/j.geomorph.2010.10.018

Luo, W., & Pederson, D. T. (2012). Hydraulic conductivity of the High Plains Aquifer re-evaluated using surface drainage patterns. *Geophysical Research Letters*, *39*(2), 1–6. https://doi.org/10.1029/2011GL050200

Maxwell, R. M., & Condon, L. E. (2016). Connections between groundwater flow and transpiration partitioning. *Science*, *353*(6297), 377–380. https://doi.org/10.1126/science.aaf7891

Maxwell, R. M., Condon, L. E., & Kollet, S. J. (2015). A high-resolution simulation of groundwater and surface water over most of the continental US with the integrated hydrologic model ParFlow v3. *Geoscientific Model Development*, *8*(1), 1–19. https://doi.org/10.5194/gmd-8-1-2015

Maxwell, R. M., & Miller, N. L. (2005). Development of a coupled land surface and groundwater model. *Journal of Hydrometeorology*, *6*(3), 233–247. https://doi.org/10.1175/JHM422.1

McGuire, V. L. (2014). Water-level changes and change in water in storage in the High Plains aquifer, predevelopment to 2013 and 2011–13. *U.S. Geological Survey Scientific Investigations Report*, (5218), 14. https://doi.org/http://dx.doi. org/10.3133/sir20145218

McGuire, V. L. (2017). Water-level changes and change in water in storage in the High Plains aquifer, predevelopment to 2015 and 2013–15. *High Plains Aquifer Water Level Monitoring Study*, 1.

Natural Resource Conservation Service, U. (2018). Watershed Boundary Dataset | NRCS. Retrieved February 6, 2019, from https://www.nrcs.usda.gov/wps/portal/nrcs/main/national/water/watersheds/dataset/

Neuman, S. P. (1990). Universal Scaling of Hydraulic Conductivities and Dispersivities in Geologic Media c is a constant , a fractal dimension where E is the topological depends only on the constants cr • and L s ,. Yet when one. *Water Resources*, *26*(8), 1749–1758. https://doi.org/10.1029/WR026i008p01749

Perkins, J. S., Gido, K. B., Falke, J. A., Fausch, K. D., Crockett, H., Johnson, E. R., & Sanderson, J. (2017). Groundwater declines are linked to changes in Great Plains stream fish assemblages. *Proceedings of the National Academy of Sciences*, *114*(28), 7373–7378. https://doi.org/10.1073/pnas.1618936114

PRISM Climate Group, O. S. U. (2018). PRISM Climate Data 30-Year Normals. Retrieved February 6, 2018, from http://prism.oregonstate.edu/normals/

Renard, P., & de Marsily, G. (1997). Calculating equivalent permiability: a review. *Advances in Water Resources*, *20*, 253–278.

Sanford, W. E., & Selnick, D. L. (2013). Estimation of Evapotranspiration Across the Conterminous United States Using a Regression With Climate and Land-Cover Data. *Journal of the American Water Resources Association*, *49*(1), 217–230. https://doi.org/10.1111/jawr.12010

Scanlon, B. R., Faunt, C. C., Longuevergne, L., Reedy, R. C., Alley, W. M., McGuire, V. L., & McMahon, P. B. (2012). Groundwater depletion and sustainability of irrigation in the US High Plains and Central Valley. *Proceedings of the National Academy of Sciences*, *109*(24), 9320–9325. https://doi.org/10.1073/pnas.1200311109

Scanlon, B. R., Ruddell, B. L., Reed, P. M., Hook, R. I., Zheng, C., Tidwell, V. C., & Siebert, S. (2017). The food-energy-water nexus: Transforming science for society. *Water Resources Research*, *53*(5), 3550–3556. https://doi.org/10.1002/2017WR020889

Scanlon, B. R., Zhang, Z., Save, H., Sun, A. Y., & Müller, H. (2018). Global models underestimate large decadal declining and rising water storage trends relative to GRACE satellite data, (3). https://doi.org/10.1073/pnas.1704665115

Schwarz, G. E., & Alexander, R. B. (1995). Soils data for the Conterminous United States Derived from the NRCS State Soil Geographic (STATSGO) Data Base. Retrieved July 18, 2018, from https://water.usgs.gov/GIS/metadata/usgswrd/XML/ussoils.xml

Shangguan, W., Hengl, T., Jesus, J. M. de, Yuan, H., & Dai, Y. (2016). Mapping the global depth to bedrock for land surface modeling. *Journal of Advances in Modeling Earth Systems*, (13 SEP 2016), 1411–1431. https://doi.org/10.1002/2016MS000660.Received

Siebert, S., Burke, J., Faures, J. M., Frenken, K., Hoogeveen, J., Döll, P., & Portmann, F. T. (2010). Groundwater use for irrigation - A global inventory. *Hydrology and Earth System Sciences*, *14*(10), 1863–1880. https://doi.org/10.5194/hess-14-1863-2010

Singh, A. (2014). Groundwater resources management through the applications of simulation modeling: A review. *Science of the Total Environment*, *499*, 414–423. https://doi.org/10.1016/j.scitotenv.2014.05.048

Sophocleous, M. A., Koelliker, J. K., Govindaraju, R. S., Birdie, T., Ramireddygari, S. R., & Perkins, S. P. (1999). Integrated numerical modeling for basin-wide water management: The case of the Rattlesnake Creek basin in south-central Kansas. *Journal of Hydrology*, *214*(1–4), 179–196. https://doi.org/10.1016/S0022-1694(98)00289-3

United States Geological Survey. (2018a). National Hydrography. Retrieved February 6, 2019, from https://www.usgs.gov/core-science-systems/ngp/national-hydrography

United States Geological Survey. (2018b). TNM Download. Retrieved February 7, 2019, from https://viewer.nationalmap.gov/basic/?basemap=b1&category=ned,nedsrc&title=3DEP View

United States Geological Survey. (2018c). USGS Map of the Principal Aquifers of the United States. Retrieved August 10, 2019, from https://water.usgs.gov/ogw/aquifer/map.html

van Beek, R. L. P. H., & Bierkens, M. F. P. (2009). The Global Hydrological Model PCR-GLOBWB : Conceptualization , Parameterization and Verification. *Department of Physical Geography, Utrecht University, Utrecht, Netherlands*.

Wada, Y., Beek, L. P. H. Van, Kempen, C. M. Van, Reckman, J. W. T. M., Vasak, S., & Bierkens, M. F. P. (2010). Global depletion of groundwater resources, *37*(September), 1–5. https://doi.org/10.1029/2010GL044571

Wada, Y., Wisser, D., & Bierkens, M. F. P. (2014). Global modeling of withdrawal, allocations and consumptive use of surface water and groundwater resources. *Earth System Dynamics Discussions*, *5*(1), 15–40.

Wood, E. F., Lettenmaier, D., Liang, X., Nijssen, B., & Wetzel, S. W. (1997). Hydrological Modeling of Continental-Scale Basins. *Annual Review of Earth and Planetary Sciences*, *25*(1), 279–300. https://doi.org/10.1146/annurev.earth.25.1.279

Wood, E. F., Roundy, J. K., Troy, T. J., Van Beek, L. P. H., Bierkens, M. F. P., Blyth, E., … Kollet, S. J. (2011). Comment on "Hyperresolution global land surface modeling: Meeting a grand challenge for monitoring Earth's terrestrial water" by Eric F. Wood et al. *Water Resources Research*, *48*(1), 1–10. https://doi.org/10.1029/2010WR010090

Zheng, C., & Gorelick, S. M. (2003). Analysis of Solute Transport in Flow Fields Influence by Preferential Flowpaths at the Decimeter Scale. *Groundwater*, *41*(2), 142–155. https://doi.org/10.1111/j.1745-6584.2003.tb02578.x

Zinn, B., & Harvey, C. F. (2003). When good statistical models of aquifer heterogeneity go bad: A comparison of flow, dispersion, and mass transfer in connected and multivariant Gaussian hydrualic conductivity fields. *Water Resources Research*, *39*(46), 137–147. https://doi.org/10.1029/2001WR001146

APPENDIX A

COMPARISON OF OBSERVED AND MODELED GROUNDWATER IN THE HIGH PLAINS

Observational data of water level depth over the High Plains aquifer were obtained through the USGS Nebraska Water Center. Data was downloaded for the entire aquifer and for each of the eight states individually, for both a “pre-development” baseline (1950-prior), and for a “post-development” case (2013). Data was spatially plotted in R-studio, and compared statistically using kernel-density plots, for the entire aquifer and for each state. This shows the heterogeneous result of pumping across the aquifer, and the variation in water table depth for the baseline case.

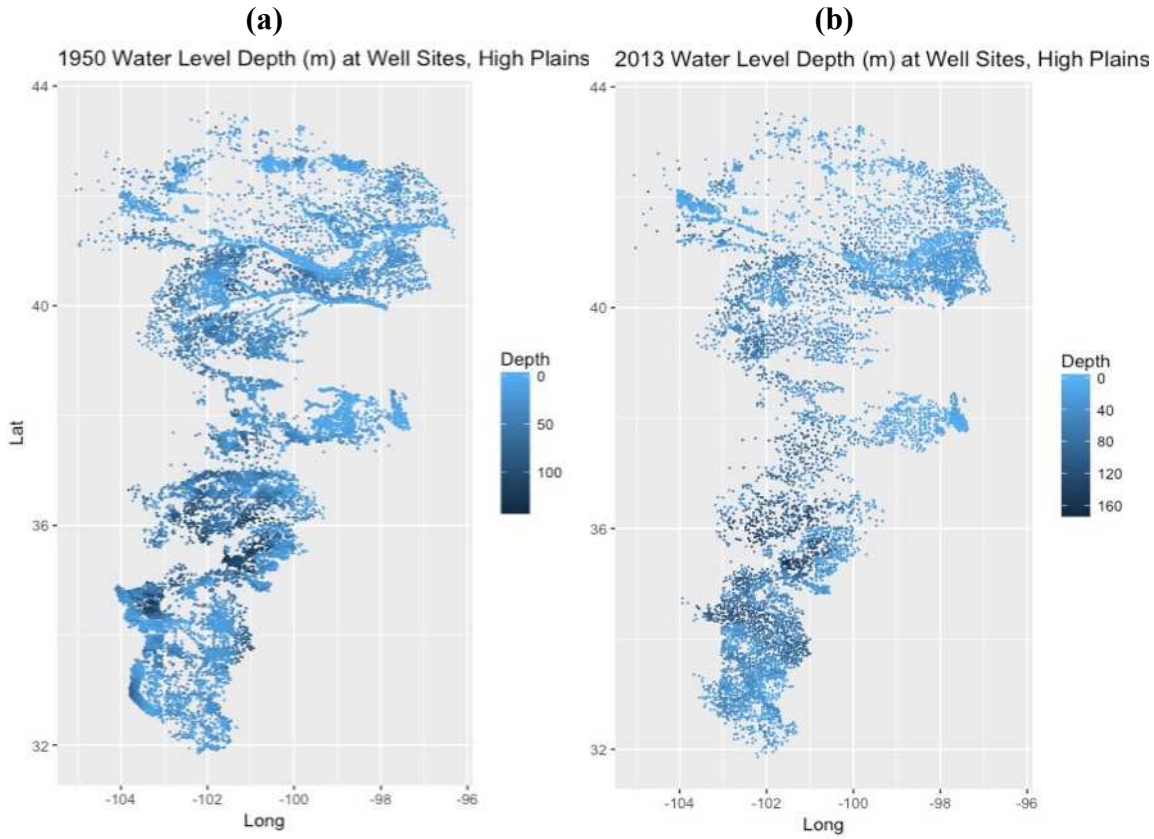

Figure A.1: Observed water table depth, in meters, across the High Plains for "pre-development" (a) and "post-development" (b).

Modeled water table depth output data was taken from Run 4 of the ParFlow CONUS model, which was run for a baseline and pumping scenario, making comparable results to USGS observation. The model data was subset over the High Plains for both the baseline and pumping runs, and spatially plotted in R-studio. The data was then statistically compared using kernel density plots to see how well the model is capturing water table depths and spatial heterogeneity compared to observational data. The results of this comparison indicate that the CONUS model is able to capture high resolution spatial heterogeneity, but shows much shallower groundwater depths that are seen in observation. This implies that the model would benefit from either deepening the subsurface boundary of the model, changing the permeability values in subsurface indicator fields to capture more local geologic heterogeneities, or a combination of the two.

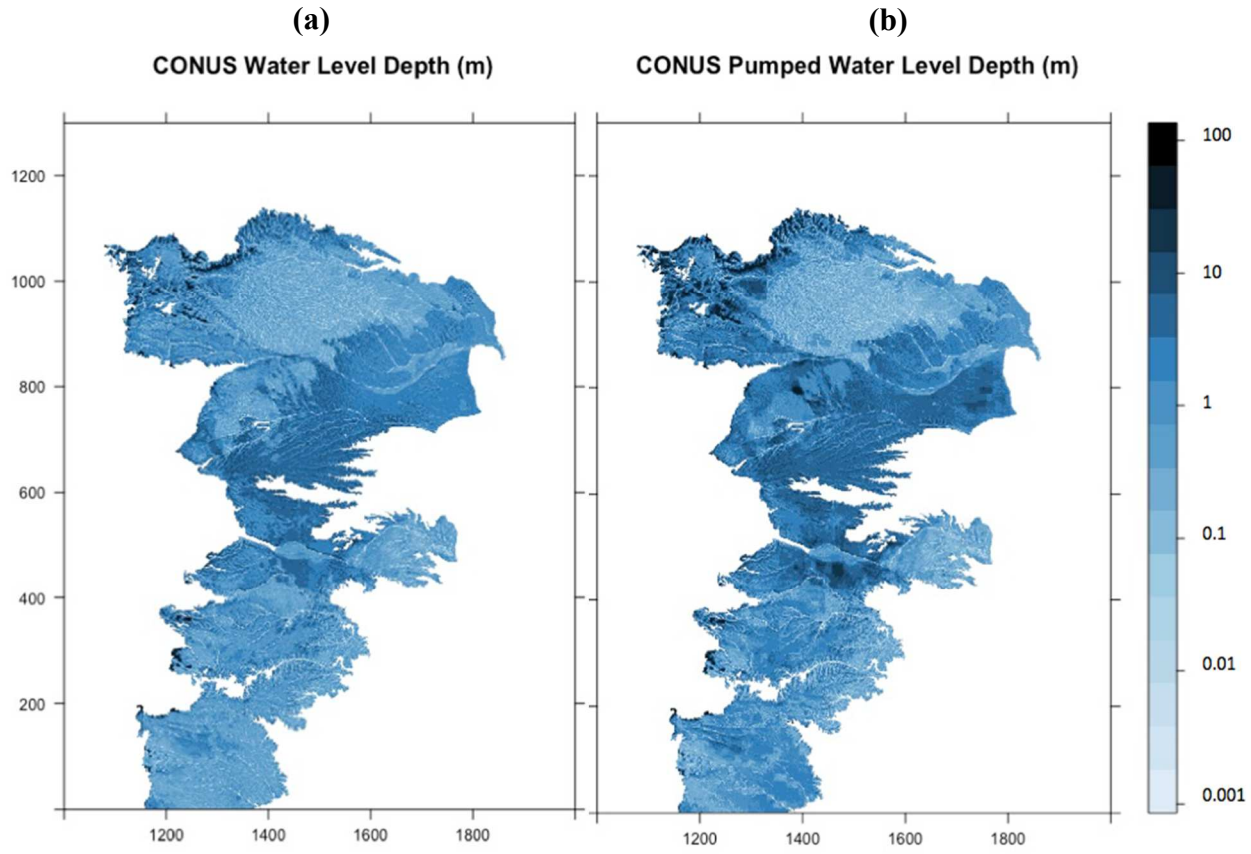

Figure A.2:Modeled water table depth, in meters, across the High Plains from "pre-development" (a) and "post-development"(b).

Figure A.2 shows that the CONUS model is predicting similar spatial water table patters across the extent of the aquifer, and is showing general agreements in the response to pumping across the domain; however, the majority of groundwater within the first 5 meters of the subsurface, while observation shows the majority of groundwater within the first 100 meters of the subsurface. This leads us to ask why the model is predicting shallow water in regions where the observed water table extends to 100 meters, even before significant anthropogenic influences. This may be attributed to historic groundwater depletion in this area, which has also lead to bias in stream flows over the high plains, compared to observation (Maxwell & Condon, 2016).

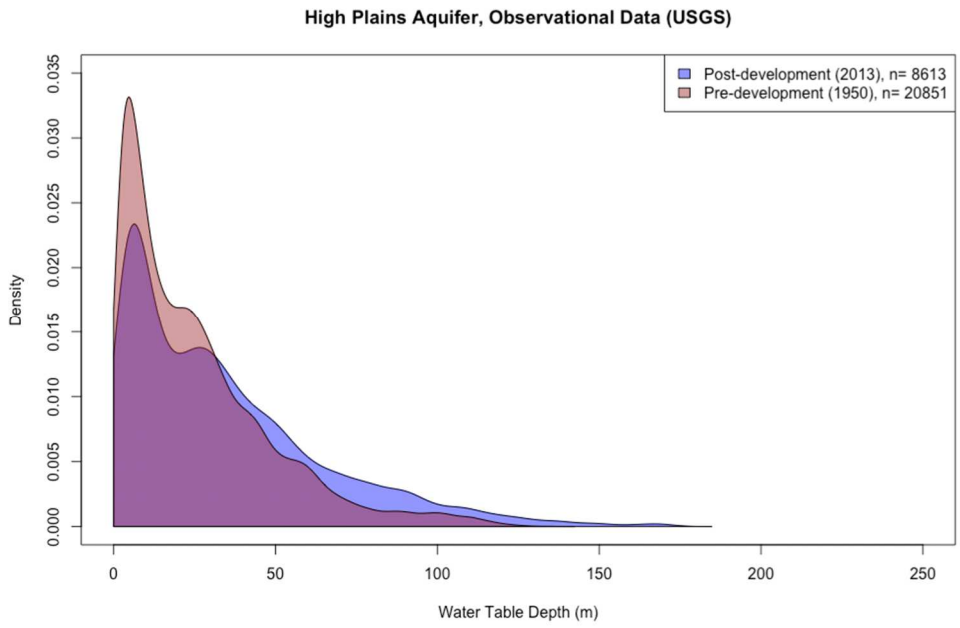

Figure A.3: Observed water table depth, in meters, across the High Plains.

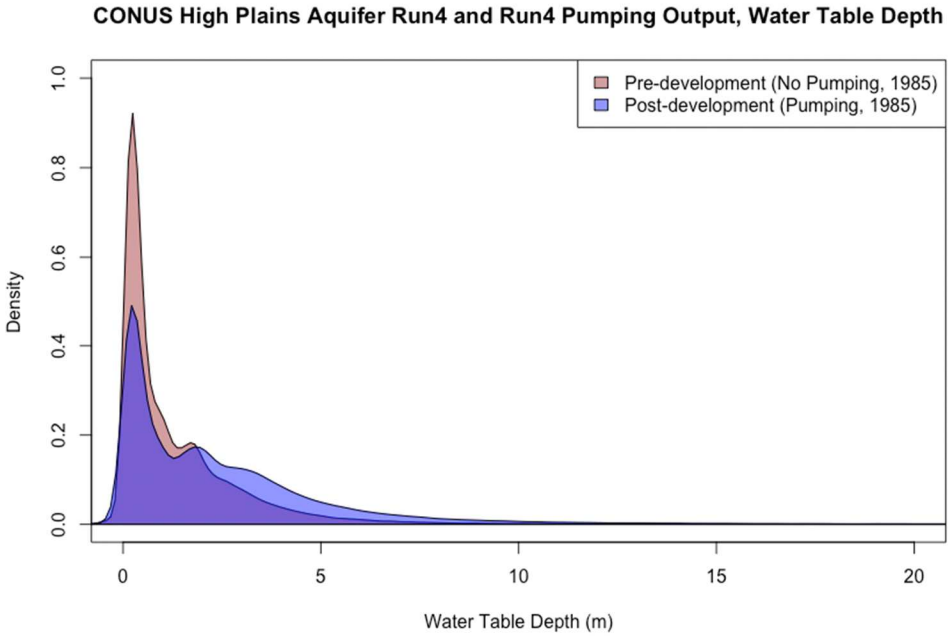

Figure A.4: Modeled distribution of water table depth, in meters, across the High Plains.

APPENDIX B

REPRODUCTING HYDRAULIC CONDUCTIVITY VALUES OVER THE HIGH PLAINS USING WATERSHED GEOMORPHOLOGY

The hydraulic conductivity values presented in Luo's 2012 were reproduced to validate the methods and test its reproducibility. This reproduction was done entirely in ArcMap 10.5 using freely available data from the USGS and PRISM Climate Group. The methods presented in his original publication were adapted to generate average subwatershed values for each of the four model parameters: valley depth, drainage density, aquifer thickness, and recharge. The following outlines the necessary processing to calculate hydraulic conductivity [m/s] using available data. This method is based upon published work from Luo et al. (2012). Either vector or raster format is acceptable.

(DEM) Digital elevation maps can be downloaded free of charge from the USGS National Map as 1deg x 1deg tiles, OR the CGIAR Consortium for Spatial Information (CGIAR-CSI) STRM Digital Elevation Data download site as five-degree by five-degree tiles. Both sources have 90-meter resolution products, and will need to be mosaicked together into one continuous DEM (Jarvis et al., 2008; United States Geological Survey, 2018b)

(Recharge) Recharge was estimated according to Luo et al. (2012). This was done by digitized the High Plains soil image from Gutentaug (1984). Next, the infiltration percentage of the soil type was assigned to each soil using a for-loop in R. The mean infiltration percentage was then found for each HUC12. Precipitation data was taken from PRISM Climate group, and averaged by HUC12. Then the precipitation was multiplied by infiltration percent for each HUC12, resulting in recharge.

(Saturated Thickness) Saturated thickness was estimated using a depth to bedrock polyline file available through the USGS GIS database. The depth to bedrock was assumed to be the maximum potential aquifer thickness. The depth to bedrock polylines were digitized and krigged to generate a continuous product. The HUC12 file was used to find the mean potential aquifer thickness using the zonal statistics tool.

(High Plains Aquifer shapefile) HPA shapefile can easily be downloaded from USGS. (United States Geological Survey, 2017).

(Watershed Boundary Data) HUC2 region through HUC12 subbasin geometry data can be downloaded from the USGS WBD website. (Natural Resource Conservation Service, 2018).

(Stream networks) USGS delineated stream network products are available for download free of charge through the national hydrography dataset (NHD) (United States Geological Survey, 2018a). This may be used in place of a watershed delineation using the constructed DEM. Watershed delineation using the DEM is not advised over the High Plains due to the Sand Hills, which will be identified incorrectly as streams. The length of stream lines in each HUC12 was found using the "Sum line lengths" tool.

After each layer is generated, use the field calculator or raster calculator to execute the following formula:

[Recharge_HUC12] / ([StreamDensity_HUC12] * [StreamDensity_HUC12]) / ([SaturatedThickness_HUC12] * [SaturatedThickness_HUC12] - ([SaturatedThickness_HUC12] - [ValleyDepth_HUC12]) * ([SaturatedThickness_HUC12] – [ValleyDepth_HUC12]))

This formula follows the original formula presented in Luo et al., 2012:

$$K = \frac{R}{D^2[H^2 - (H-d)^2]}$$

The map below compares the hydraulic conductivity estimated from this test to the results from Luo et al. 2012. There is some spatial discrepancy, however these results give promise that this will be an effective method for estimating hydraulic conductivity across the continental US.

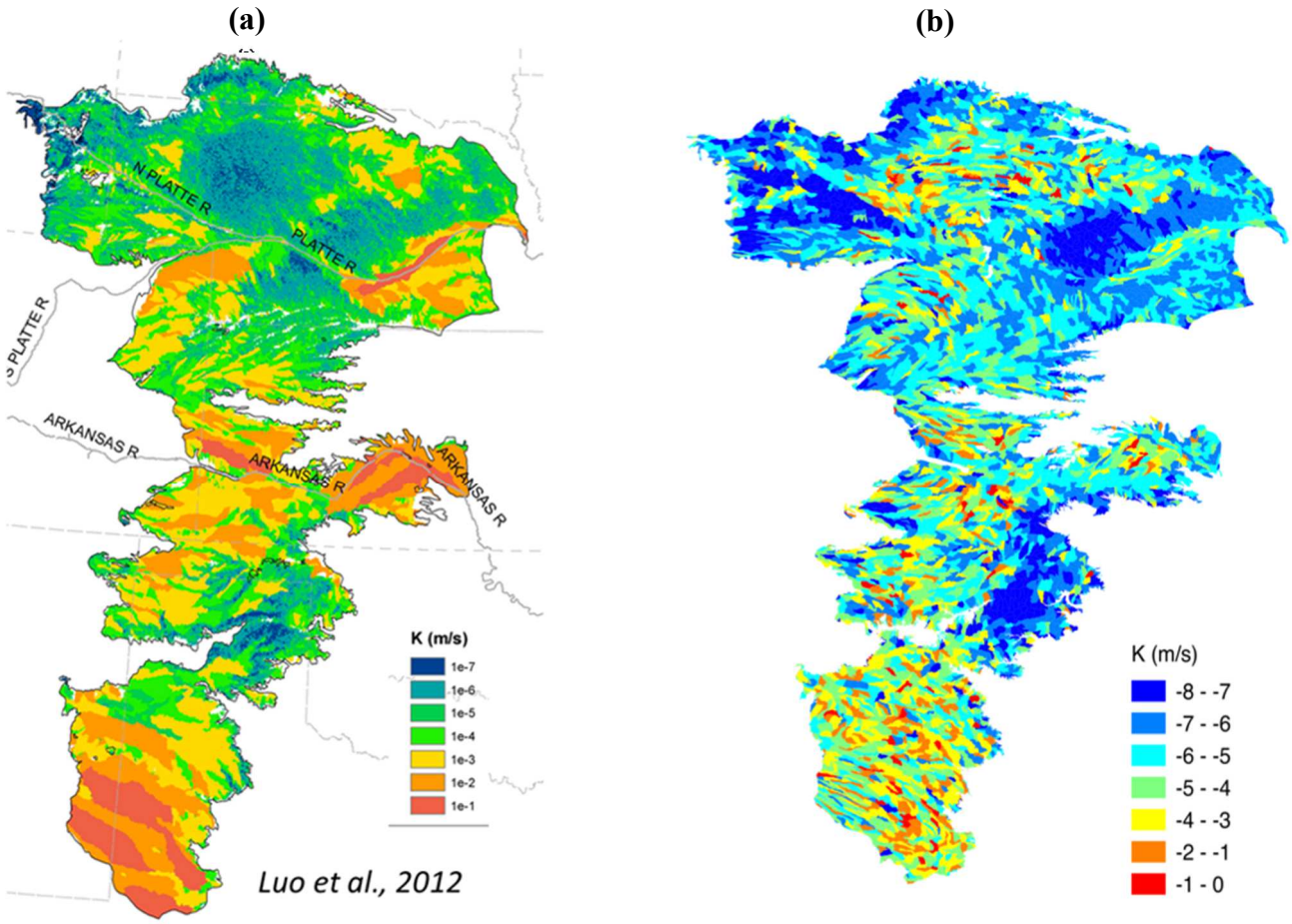

Figure B.1: Results from Luo et al 2012 compared to the preliminary results of our estimate across the High Plains.

APPENDIX C

INPUT PARAMETERS FOR HYDRAULIC CONDUCTIVITY

CALCULATION OVER THE CONTINENTAL US

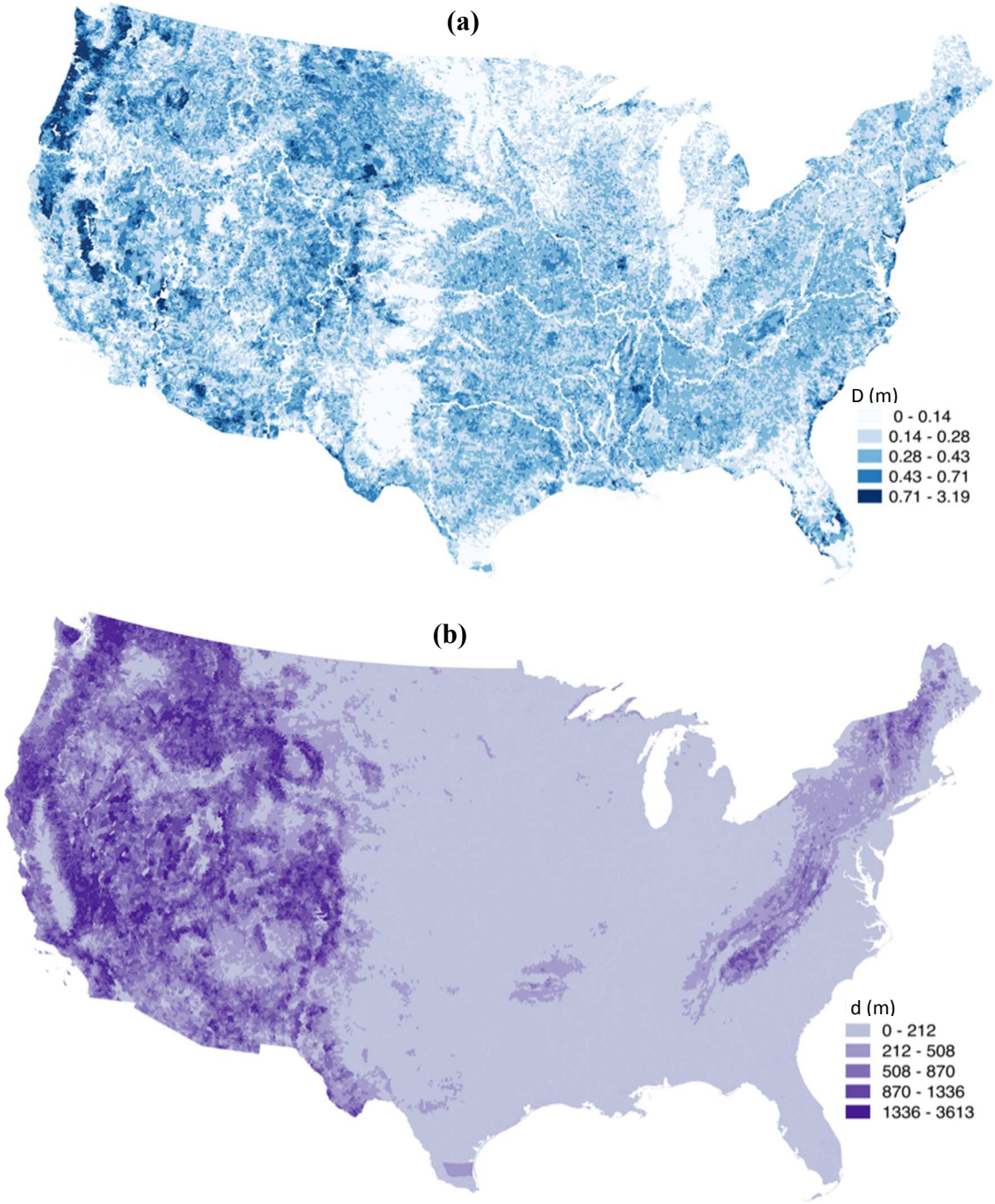

Figure C.1: Parameters used to estimate hydraulic conductivity using the methodology: (a) Drainage density, D; (b) Valley depth, d; (c) Aquifer thickness, H; (d) Precipitation, P; (e) Infiltration percent, I; (f) Evapotranspiration, ET.

(c)

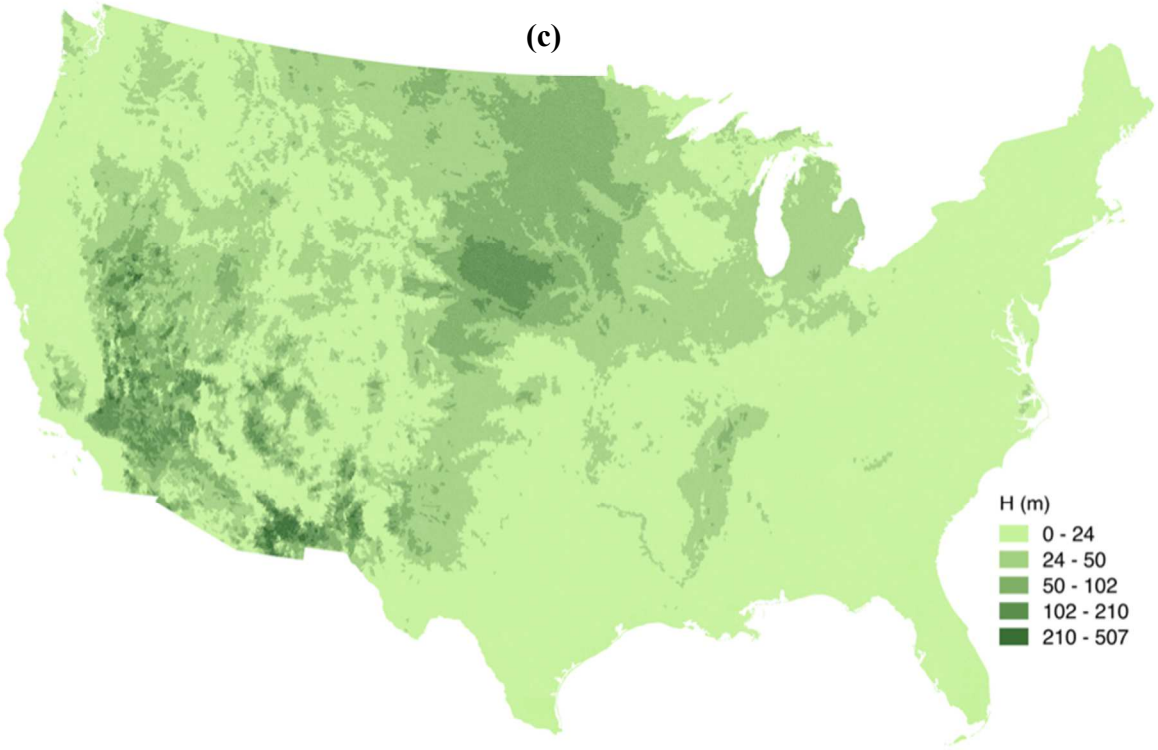

(d)

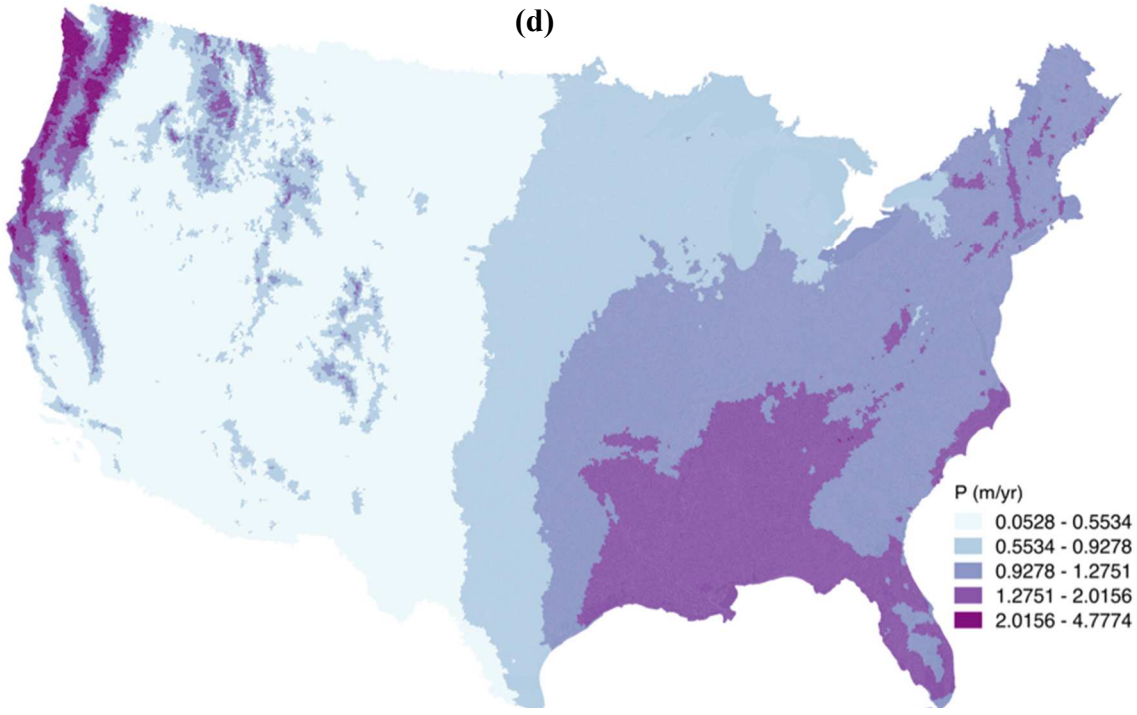

Figure C.1: Continued

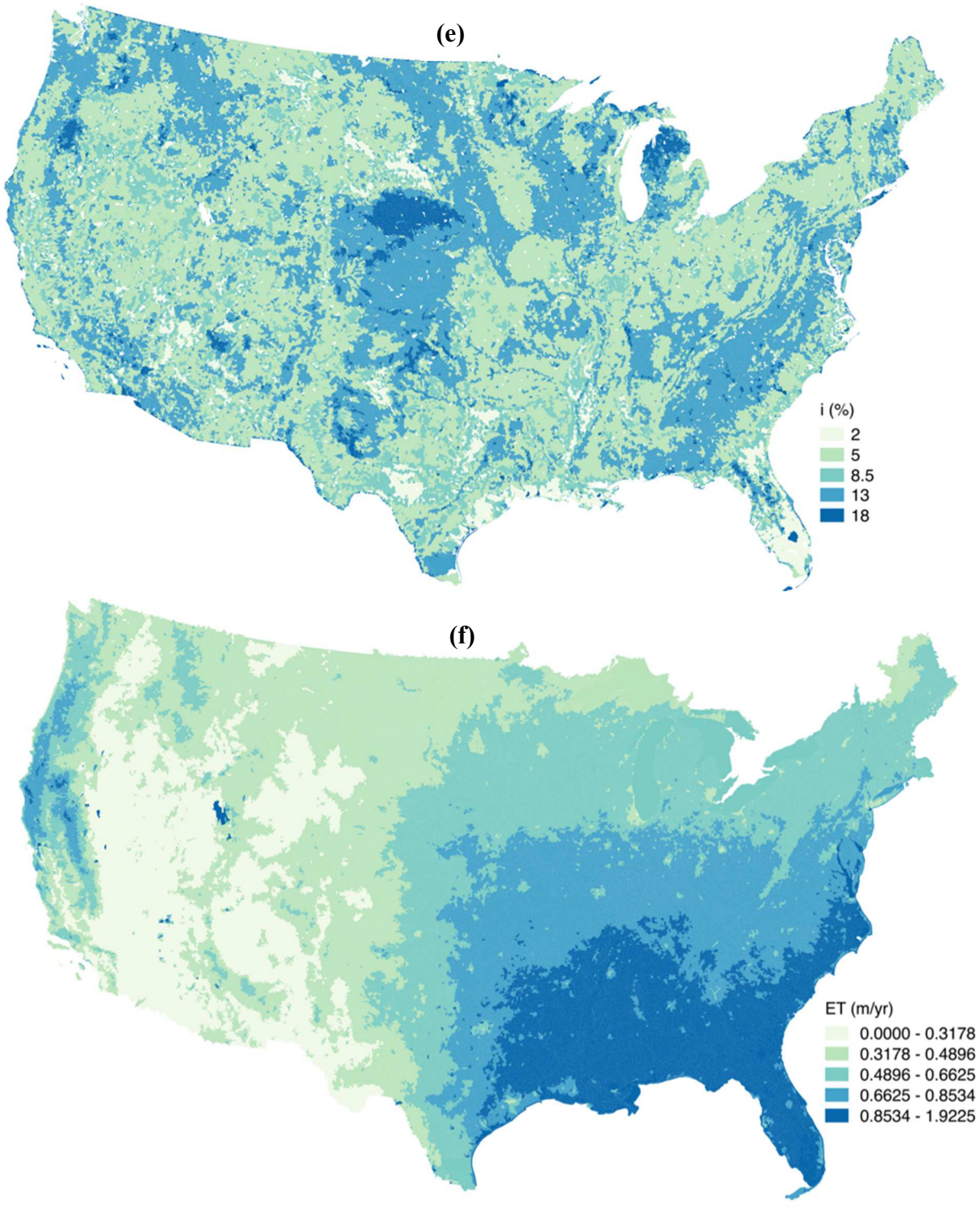

Figure C.1: Continued